Marine and Petroleum Geology 155 (2023) 106403

Contents lists available at ScienceDirect

Marine and Petroleum Geology

journal homepage: www.elsevier.com/locate/marpetgeo

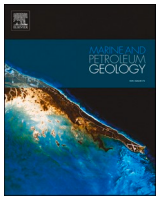

New methods to reconstruct paleo-oil and gas compositions and *P-T* trapping conditions of hydrocarbon fluid inclusions in sedimentary basins

Hongwei Ping [a,*], Régis Thiéry [b], Honghan Chen [a], Honglin Liu [c]

[a] Key Laboratory of Tectonics and Petroleum Resources (China University of Geosciences), Ministry of Education, Wuhan, 430074, China
[b] UMR 6524 'Magmas et Volcans', Université Clermont Auvergne, 63000, Clermont-Ferrand Cedex, France
[c] Research Institute Petroleum Exp. & Dev., Petrochina, Beijing, 100083, China

ARTICLE INFO

Keywords:
Petroleum inclusion
Gas condensate
Paleo-pressure
Thermodynamics modeling
PVT modeling

ABSTRACT

Accurate predictions of fluid composition and *P-T* trapping condition of hydrocarbon fluid inclusions (HFIs) is crucial to understand complex oil and gas charging history and accumulation mechanism. However, traditional *P-T* prediction methods are not enough powerful to get reliable results because of difficulty in direct composition measurement and great uncertainties in indirect composition prediction for single HFI. In this study, we collected 296 crude oil and 983 gas condensate fluids to develop new composition and trapping pressure (P_t) prediction models. Based on the measured fluid composition, saturation pressure (corresponding to homogenization pressure, P_h) and volume data, we firstly calibrate the P_h, the degree of bubble filling (F_v, at 20 °C) and isochores predictions for the measured fluids through matching saturation pressure and volume calibration and then established a standard fluid database with fluid composition, P_h, F_v and P_t. For the first time, a new hydrocarbon fluid composition prediction model was developed which is only function of F_v and homogenization temperature (T_h) of HFIs. The new composition model allows directly predicting the entire fluid compositions from methane (C_1) to heptane plus (C_{7+}) fractions in HFI based on F_v and T_h. Furthermore, we developed different P_t prediction models for varying fluid compositions and phase states of HFIs. For oil-bearing fluid inclusions which homogenize into liquid phase (OFI_L) methane molar content is the only variable that is needed to predict P_t with a high degree of accuracy (8.2–12.3% for average absolute deviation, AAD). However, for gas condensate-bearing fluid inclusions (GCFI), more composition (C_1–C_{7+}) together with the physical property (molecular weight and specific gravity) of C_{7+} composition must be incorporated into the prediction model to obtain a better prediction accuracy of P_t. The new P_t prediction models give prediction accuracy of 11.2–17.6% (AAD) for $GCFI_L$ (homogenizing into liquid phase), and 15.9–22.8% (AAD) for $GCFI_G$ (homogenizing into gas phase). Our new composition and P_t prediction models can give the best and fastest predictions of hydrocarbon fluid composition and trapping condition and are of great significance for petroleum charging history reconstruction in sedimentary basins.

1. Introduction

Hydrocarbon fluid is one of the most import organic mineral resources and widely distributes in sedimentary basins. Reconstructing paleo-hydrocarbon composition and pressure-temperature (*P-T*) conditions of source rocks and reservoirs are vital for understanding hydrocarbon fluid generation, migration, accumulation (Hubbert, 1953; Schowalter, 1979; England et al., 1987). Tiny hydrocarbon fluids including crude oil, gas condensate and natural gas can be trapped in rock minerals as hydrocarbon fluid inclusions (HFIs) in a wide range of geological processes or events. Fluid inclusions generally represent original samples of paleo-fluid and provide the best available methods to reconstruct the temperature, pressure and composition of the fluid at the time of trapping in conjunction with mineral paragenetic studies (Roedder, 1984). Therefore, HFIs have been widely used in oil and gas exploration to reconstruct the *P-T* trapping conditions of the paleo-petroleum fluid as well as its source and thermal maturity (see Munz, 2001; Volk and George, 2019 for a review).

One of the important preconditions for *P-T* reconstruction of HFIs is to know the molar composition of trapped hydrocarbons from gas to high molecular weight liquid hydrocarbon (Munz et al., 1999b). However, it is usually difficult to measure the detailed composition of HFIs

* Corresponding author.
E-mail address: Hongwei.Ping@cug.edu.cn (H. Ping).

https://doi.org/10.1016/j.marpetgeo.2023.106403
Received 20 December 2022; Received in revised form 25 March 2023; Accepted 30 June 2023
Available online 7 July 2023

directly because of very small size (micron level) and limited abundances of HFIs trapped within minerals. The composition of HFIs can be obtained by on-line or off-line crush technology for single generations (Ping et al., 2020b) or groups of petroleum inclusions (Karlsen et al., 1993; George et al., 1997), or by destructive in-situ laser ablation coupled with gas chromatograph-mass spectrometric (GC–MS) analysis for single petroleum inclusion (Hode et al., 2006; Volk et al., 2010; Zhang et al., 2012) or by directly non-destructive fluorescence measurement of single petroleum inclusion (Ping et al., 2020a). A direct on-line crushing method is suitable for the analysis of C_{12-} hydrocarbons especially for the volatile compounds and *n*-alkanes (Munz et al., 1999b; Volk et al., 2002; George et al., 2008), while the C_{12+} hydrocarbons including aromatic hydrocarbons and biomarkers are better obtained by an off-line crushing method (George et al., 1998, 2007). Furthermore, it may result in hydrocarbon mixing of multiple-generation of HFIs (e.g., methane gas mix from varying generations of oil inclusions or/and methane-bearing gas inclusions) during conventional crushing (Tseng et al., 1999; George et al., 2001; Munz, 2001) which significantly affect the *PVT* property calculation of single HFI. Up to now, current techniques are still not enough developed to analyze the composition of single HFI by on-line laser ablation coupled with GC-MS or time-of-flight secondary ion mass spectrometry (ToF-SIMS), and to constrain the *PVT* calculation models for HFIs (Volk et al., 2010; Zhang et al., 2012; Siljeström et al., 2013, 2021). Therefore, an iterative method using homogenization temperature (T_h) and the degree of bubble filling (F_v) of HFIs coupled with *PVT* phase equilibrium calculation has been proposed to indirectly obtain the fluid compositions in HFIs (Aplin et al., 1999; Thiéry et al., 2000, 2002). The F_v of HFI can be determined using Confocal Laser Scanning Microscopy (CLSM) in reflected-light mode (Pironon et al., 1998; Aplin et al., 1999) or using a conventional petrographic microscope illuminated by transmitted white light (Bakker and Diamond, 2006). However, only the two parameters (T_h and F_v) cannot uniquely constrain the compositions of HFIs (Thiéry et al., 2002). Usually, a reservoir fluid composition (Aplin et al., 1999, 2000; Tseng et al., 1999; Tseng and Pottorf, 2002; Liu et al., 2003; Munz et al., 2004) or an α-β model composition (Teinturier et al., 2002; Thiéry et al., 2000, 2002; Bourdet et al., 2012) are used as initial composition for iterative computations. The final fluid compositions are obtained once the calculated F_v value equals to the measured one under the same temperature (usually room temperature). The *P-T* trapping condition prediction largely depends on the selection of reservoir fluid composition but usually it is difficult to correlate the compositions of reservoir fluids to fluid inclusion oils. Because any post-trapping composition modifications (e.g., biodegradation, oil cracking, gas injection and gas exsolution) could greatly change the reservoir fluid compositions which results in significant difference in compositions between the fluid inclusion oils and reservoir fluids. Although the α-β model can provide a series of various initial compositions for iterative calculations, the final fluid composition must be determined through the constraint of a third parameter, e.g., petroleum types (Bourdet et al., 2008; Ping et al., 2012), API gravity (Tseng and Pottorf, 2002; Ping et al., 2017a, 2019), gas oil ratio (Thiéry et al., 2002), methane molar content determined by Fourier Transform Infrared (FT-IR) microspectroscopy (Pironon et al., 2001; Bourdet et al., 2012, 2014) or F_v variation in different temperatures (Ferket et al., 2011). Among these parameters the methane molar content is the most important one as it directly related to fluid composition and the homogenization pressure (P_h) of HFI (Ping et al., 2011). Ping et al. (2013a) evaluated the accuracy of different trapping pressure (P_t) prediction methods (Aplin et al., 1999; Thiéry et al., 2002) using measured fluid and calculated equivalent fluid derived from petroleum type determination (Bourdet et al., 2008; Ping et al., 2012). They showed that the average absolute deviation (AAD, $\frac{1}{N}\sum_{i=1}^{N}\left|\frac{P_{cal}-P_{exp}}{P_{exp}}\right| \times 100\%$, where N is the number of data points and P_{cal} and P_{exp} are calculated pressure and experimental pressure, respectively) of P_t predication varied from 8 to 14% to about 20% constrained by true fluid and equivalent fluid, respectively. In addition, because of complicated *PVT* phase equilibrium calculations these methods largely rely on professional softwares (e.g., VTFLINC, PVTsim, PIT and FIT-Oil) which significantly limit their application and further modifications.

Ping et al. (2013a, 2013b) systematically improved the prediction accuracy of P_h and F_v of HFI and finally proposed a direct prediction formula of P_t with only variable of methane molar content, which is very easy to use compared to other professional softwares. Furthermore, the new method has better prediction accuracy with AAD ranging from 6% to 15% (Ping et al., 2013b), if true methane molar content is known or methane molar content is indirectly determined from equivalent fluid, respectively. However, the Ping et al. (2013b) method is derived from crude oil samples and is not applicable for gas condensate and natural gas inclusions. Indeed, the *PVT* phase behavior of gas condensate fluid is more complex than that of crude oil. To only know the molar contents of methane is sufficient to make good predictions of P_h of crude oils and the trapping conditions of oil inclusion (Ping et al., 2011, 2013b). For obtaining good predictions of dew point pressures (equivalent to P_h) one usually needs more than ten additional variables including molar content of N_2, CO_2, H_2S, C_1–C_{7+}, and the specific gravity (SG) and molecular weight (MW) of C_{7+} composition (Nemeth and Kennedy, 1967; Elsharkawy, 2002b; Shokir, 2008; Al-Dhamen and Al-Marhoun, 2011; Kamari et al., 2016; Haji-Savameri et al., 2020). In fact, all these parameters during *PVT* thermodynamic modeling of gas condensate are difficult to obtain, which greatly increases the difficulty in predicting *P-T* trapping conditions of gas condensate inclusions.

In this study, we focus on varying hydrocarbon fluids from crude oil to gas condensate and wet gas. To obtain accurate predictions of fluid compositions and *P-T* trapping conditions of HFIs we collected more than 1200 published fluid compositions worldwide and established a new predictive model of fluid composition which is only related to the T_h and F_v of HFI. Furthermore, we improved the predictions of P_h and F_v of crude oil and gas condensate fluids and proposed new methods to directly calculate the *P-T* trapping conditions of crude oil and gas condensate inclusions using only the T_h and F_v of HFI. Finally, the prediction accuracies of the new methods have been evaluated. Our new methods make the prediction of paleo-oil and gas composition and *P-T* conditions of hydrocarbon fluids easier and can obtain a good predictive precision of *P-T* condition to 5–10 km burial depths (equivalently oil-gas generating window depending on geothermal gradient) in sedimentary basins.

2. Materials and methods

2.1. Basic principle and conditions

The *P-T* condition reconstruction of HFI is based on the precondition of simultaneously trapping of immiscible hydrocarbon and aqueous fluids as fluid inclusions in diagenetic minerals. If the hydrocarbon and coeval aqueous fluid inclusions meet the “Roedder’s Rules” (Roedder, 1984), the intersection point of the isochores of the two immiscible fluids in single phase zone can constrain the *P-T* trapping condition of HFI (Haszeldine et al., 1984; McLimans, 1987; Munz et al., 1995; Pironon, 2020). Fig. 1 shows an example of a normal oil inclusion coeval with methane-bearing aqueous fluid inclusions with various methane concentration under different trapping conditions. Generally, three types of trapping conditions may be encountered under geological conditions 1) both the oil inclusion and aqueous inclusion are unsaturated with methane which are trapping at point A in Fig. 1 and 2) the oil inclusion is unsaturated with methane, but the aqueous inclusion is saturated with methane and they are trapped at point B in Fig. 1 and 3) both the oil inclusion and aqueous inclusion are saturated with methane, and they are trapped at point C in Fig. 1. For the first case, the T_{hs} of oil inclusion (T_h^C in Fig. 1) and aqueous inclusion (T_h^D in Fig. 1) are lower than their true trapping temperature (T_t^A in Fig. 1) and only the isochores of oil inclusion (line AA’ in Fig. 1) and aqueous inclusion (line AD in

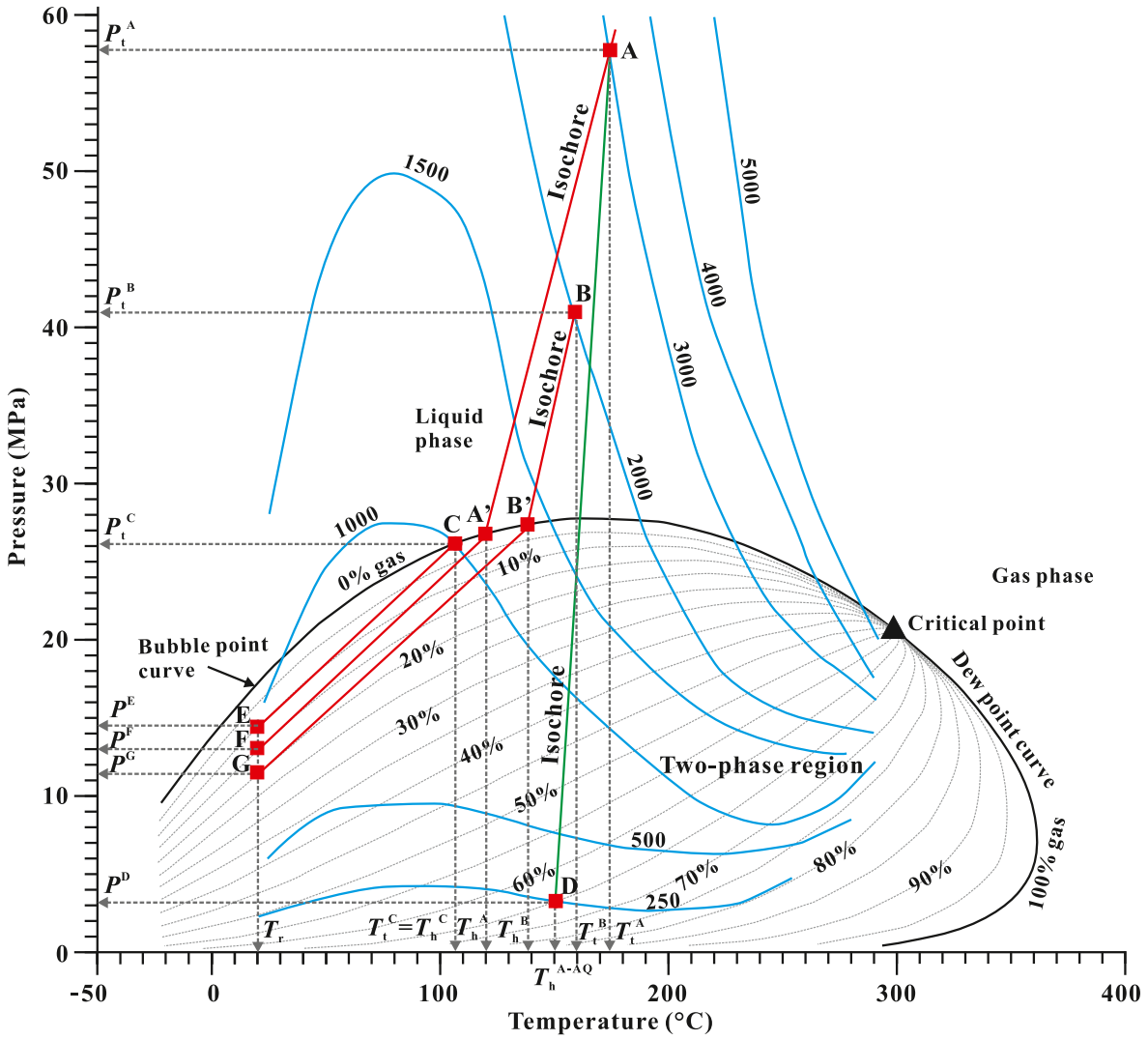

Fig. 1. Basic principle of *P-T* trapping condition reconstruction of HFI based on the isochores intersection of a HFI and cogenetic aqueous fluid inclusions with varying methane concentration. The black solid curve is a typical *P-T* phase diagram of an oil inclusion including bubble point and dew point curves separating by a critical point. The gray dash curves within the two-phase region are the volume percentage of gas phase in the whole hydrocarbon phases. The blue solid curves are the solubility (ppm) curves of methane in a NaCl–H_2O system (150000 ppm NaCl) (Hanor, 1980). Points A, B and C are three assumed *P-T* trapping conditions of an oil inclusion with constant compositions and its coeval aqueous fluid inclusion with varying methane concentration. Point A means that the oil inclusion and an aqueous fluid inclusion with methane concentration of 250 ppm were trapped simultaneously at T_t^A and P_t^A. Please note both the oil and aqueous fluid inclusions were not saturated with methane at the time of trapping and the red line AA' and green line AD are the isochores of oil inclusion and aqueous fluid inclusion, respectively. The T_h^A and T_h^{A-AQ} are the T_h of oil inclusion and aqueous fluid inclusion, respectively. Point B (T_t^B, P_t^B) means the oil is not saturated with methane while the aqueous fluid inclusion is saturated with methane (methane concentration is 2000 ppm) at the time of trapping. The red line BB' is the isochore of oil inclusion and the T_h of oil inclusion is T_h^B, while the T_h of aqueous fluid inclusion equals to its trapping temperature ($T_t^B = T_h^B$) as it is saturated with methane. Point C (T_t^C, P_t^C) means both the oil and aqueous fluid inclusions are saturated with methane (methane concentration is 1000 ppm) at the time trapping and the T_h of oil inclusion and aqueous fluid inclusion and trapping temperature are equal to each other. The red lines CE, A'F and B'G are the isochores of the oil inclusion in the two-phase region for trapping conditions C, A and B, respectively. Points E, F and G indicates the internal pressures (P^E, P^F and P^G) and the corresponding degree of bubble filling (F_v) values (10%, 15% and 20%) of the inclusion at room temperature (T_r) for trapping conditions C, A and B, respectively.

Fig. 1) are known, the trapping pressure can be determined by the intersection point of the two isochores (point A in Fig. 1). For the second case, because the aqueous inclusion is saturated with methane, its T_h equals to trapping temperature (T_t^B in Fig. 1) and the trapping pressure (P_t^B) can be constrained by only the isochore of oil inclusion (BB' in Fig. 1) and the T_h of aqueous inclusion. For the last case, both the T_{hs} of oil and aqueous inclusions equal to their trapping temperature (point C in Fig. 1) and the P_h of oil inclusion is the trapping pressure. This illustrates that for obtaining *P-T* conditions of HFI the saturation degree of the oil and coeval aqueous fluid inclusions should be known first.

The T_h of HFI is generally lower than its trapping temperature depending on its gas saturation degree and trapping pressure and could vary from more than 100 °C to even negative values in inclusions trapped under deeply buried conditions (Pironon and Bourdet, 2008; Ping et al., 2017a, 2017b). The difference in T_h between hydrocarbon and cogenetic aqueous inclusions is an important indicator for the saturation degree of the hydrocarbon fluids at the time of trapping (Munz et al., 1999a; Tseng and Pottorf, 2002; Vityk et al., 2002). For examples, if oil is saturated with respect with gas, the T_h of oil inclusion approaches the T_h of the coexisting aqueous inclusions, which is more often occurring in the situations of gas charge into oil reservoir or trapping conditions where gas-liquid phase separation occurs due to

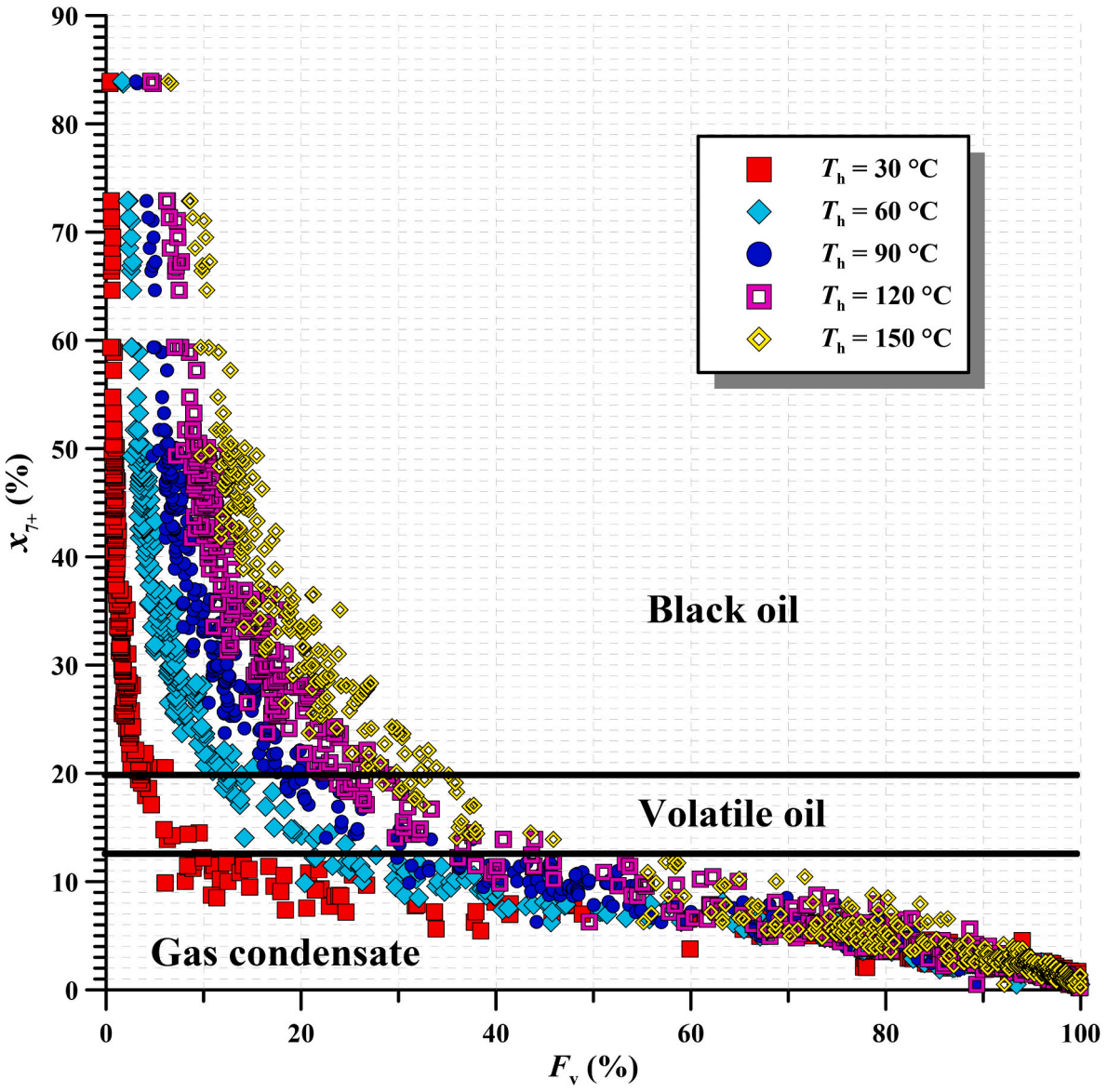

Fig. 2. Relationship between mole percent of C_{7+} cut (x_{7+}) of the measured fluid and the degree of bubble filling, F_v (calculated at 20 °C) at varying homogenization temperature (T_h) of HFI.

migration into shallower reservoirs. Under this situation, the T_h and P_h of HFI are equivalent to trapping temperature and pressure (Ping et al., 2019). The T_h of cogenetic aqueous inclusions generally represent the minimum temperature of trapping (Roedder, 1984). The difference between the T_h of aqueous inclusions and its true trapping temperature (T_t) depends on dissolved methane content in aqueous inclusions. If an aqueous inclusion is free of dissolved methane, a pressure correction should be applied to obtain a more accurate trapping temperature and the true trapping temperature could be from several tens to one hundred of degrees higher than its T_h relying on its trapping pressure in NaCl–H_2O system (Potter, 1977). For aqueous fluid inclusions containing dissolved methane, a pressure correction can result in an erroneously high estimate for trapping temperature without more detailed knowledge of aqueous compositions and methane contents (Hanor, 1980). Experiments and theoretical calculations indicate that the solubility of methane in aqueous solutions at oil window *P-T* conditions is always low, typically below 0.3 mol/kg water in NaCl aqueous solutions (Duan et al., 1992). Methane can be generated in sediments from a wide range of thermal maturity, from biogenic dry gas, oil-associated gas to wet and dry gas stages. Significant amounts of methane can be generated during transformation of kerogen into oil and gas (Tissot and Welte, 1984). Therefore, methane is expected to be saturated in formation water in equilibrium with hydrocarbons, where methane-bearing hydrocarbon fluids and aqueous fluids coexist in the same pore space. The methane concentration in the aqueous solutions can be determined by Raman spectrometry (Dubessy et al., 2001; Guillaume et al., 2003; Caumon et al., 2014; Le et al., 2020) or microthermometric measurements (Mao et al., 2013; Raimbourg et al., 2014). The T_h of aqueous inclusions could be approximate to or may be slightly lower (1–4 °C) than the trapping temperature for trapped aqueous fluid equilibrated with a hydrocarbon-rich gas or liquid (Thiéry, 2006). Therefore, the T_h of cogenetic aqueous fluid inclusion with HFI has been generally interpreted as an approximation of trapping temperatures (Nedkvitne et al., 1993; Alderton and Bevins, 1996; Tseng and Pottorf, 2002; Ping et al., 2017a). In addition, the more methane-unsaturated aqueous inclusions are the lower is their T_h of aqueous inclusions. From this view, the T_h of aqueous inclusions could represent varying methane concentration throughout inclusions entrapment (Narr and Burruss, 1984). Once the

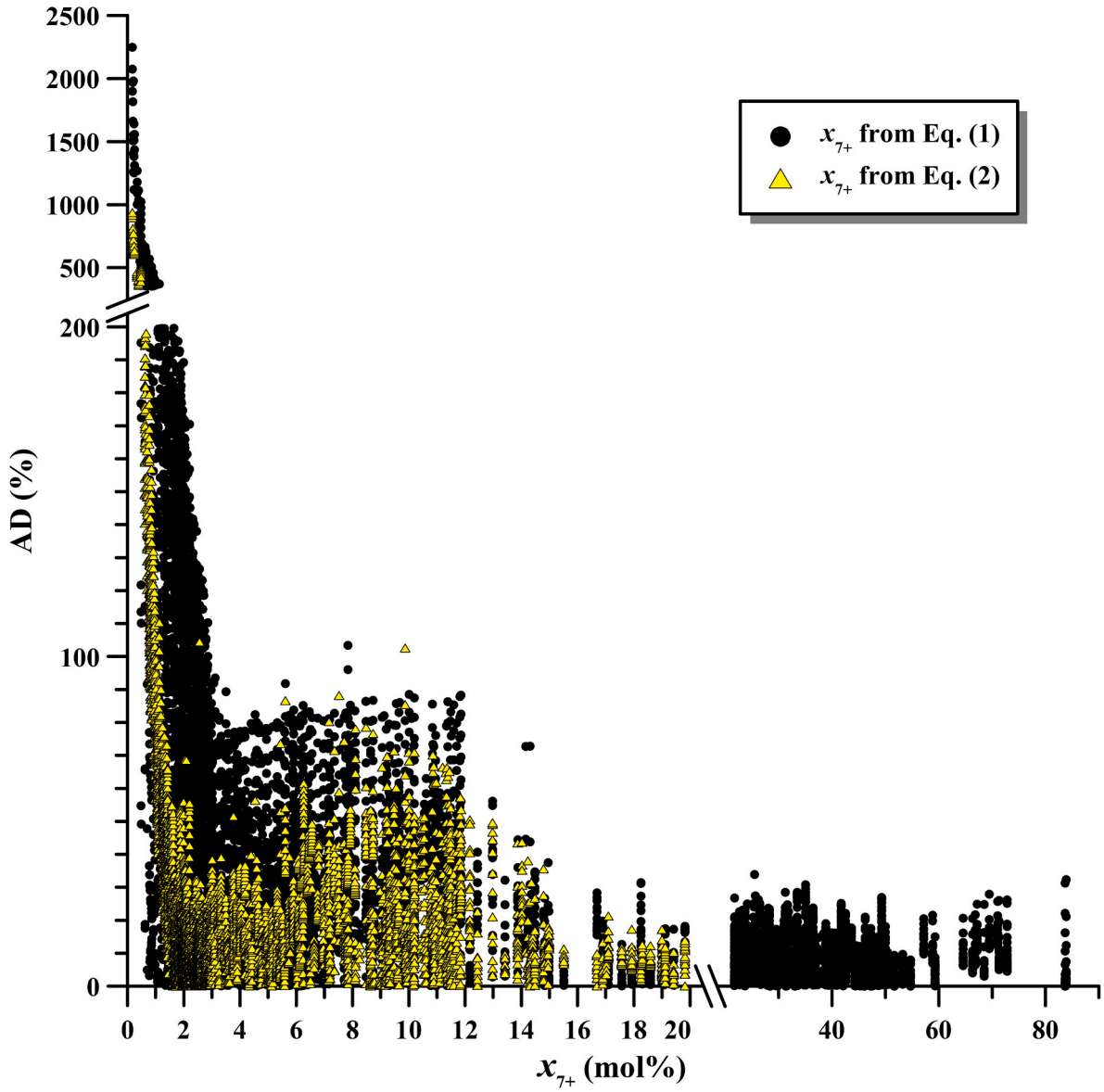

Fig. 3. Relationship between the absolute deviation (AD) of predicted mole percent of C_{7+} cut (x_{7+}) based on Eq. (1) and Eq. (2) and the measured x_{7+} for all the crude oil and gas condensate fluids.

methane concentration, salinity and fluid composition of aqueous inclusions are known, the crosscutting isochore technique performed on the HFI and coeval aqueous inclusions can be used to obtain the true trapping conditions for methane unsaturated aqueous fluids (Pironon and Bourdet, 2008; Bourdet et al., 2012; Pironon, 2020).

To sum up, the *P-T* trapping conditions of HFIs can be determined by the isochores intersection of HFI and coeval methane unsaturated aqueous inclusions, or by only the isochore of HFI and T_h ($T_h = T_t$) of coeval aqueous fluid inclusion if the aqueous fluid inclusions are saturated with methane. In this study, we only focus on the HFIs and the *P-T* trapping conditions reconstruction of HFIs is based on the isochore of HFI with assumed T_t. Generally, the isochore of HFI can be calculated through equation of state (EoS) if the molar composition and T_h of HFI are known. As discussed in Section 1 the pseudo-compositions of HFI are generally obtained by matching the measured T_h and F_v of HFI with the calculated values with changing of initial compositions from reservoir fluid or model fluid (Aplin et al., 1999; Thiéry et al., 2000, 2002). The greatest disadvantage of this inverse modeling method is that the accuracy of the calculated P_h, F_v and the resultant isochors during iteration are unknown. Here we use a forward modeling method which is similar with that of Ping et al. (2011, 2013b) to obtain accurate P_h, F_v and isochors of HFIs based on a large number of measured hydrocarbon fluid compositions and *PVT* properties (e.g., bubble/dew point pressure, molar volume of liquid and gas phase) experimentally. In other words, a lot of approximately standard HFI with known composition, P_h, F_v and trapping pressure were used. Finally, we apply these data to establish the empirical equations for calculation of hydrocarbon fluid composition and *P-T* trapping conditions from crude oil to natural gas.

2.2. Data collection

We collected a total of 1279 measured hydrocarbon fluid composition and saturation pressure (equivalently P_h ($T = T_h$)) data from publications including 296 crude oil and 983 gas condensate and wet gas fluids. The ranges of molar content of N_2, CO_2, H_2S, C_1–C_{7+} and molecular weight and density of C_{7+}, and the temperature (equivalently, T_h) and saturation pressure (equivalently, P_h) from crude oil and natural gas fluids are listed in Table 1 and Table 2, respectively. The crude oil

Table 1
The range of experimental molar composition (%), temperature, and bubble point pressure of crude oil used in this study. SG_{7+}: specific gravity of C_{7+} composition; MW_{7+}: molecular weight of C_{7+} composition (g/mol); T: temperature which is equivalent to homogenization temperature (T_h); P_b: bubble point pressure which is equivalent to homogenization pressure (P_h); N: number.

Reference	N_2 (mol%)	CO_2 (mol%)	H_2S (mol%)	C_1 (mol%)	C_2 (mol%)	C_3 (mol%)	C_4 (mol%)	C_5 (mol%)	C_6 (mol%)	C_{7+} (mol%)	SG_{7+}	MW_{7+} (g/mol)	T (°C)	P_b (MPa)	N
Agarwal et al. (1990)	0.33	3.03	0	41.33	8.89	5.95	4.12	2.66	0	33.69	0.848	200.0	93.33	22.07	1
Ahmadi et al. (2014)	0.08–0.15	0.56–1.90	0.01–0.16	3.44–46.57	1.88–8.90	3.45–5.62	4.49–7.00	4.03–9.00	4.07–5.92	24.11–68.67					2
Ahmed (1989)	0–1.64	0–0.44	0	28.40–42.00	4.64–8.00	2.46–10.48	2.00–8.40	1.00–3.82	4.00–5.46	35.97–48.24	0.82–0.84	225.0–255.0	55.00–82.22	11.78–22.41	3
Ali and El-Banbi (2015)	0.20–3.95	0.05–0.77	0	37.45–72.09	6.36–10.52	6.23–7.78	4.07–8.43	1.77–5.91	1.28–4.61	7.23–21.30			104.44–109.44	18.39–34.85	2
Almehaideb et al. (2000)	0.13–0.47	1.82–2.64	0	17.74–28.70	5.04–6.57	5.70–6.70	5.27–7.33	4.51–6.32	4.29–5.49	41.67–51.49		211.8–219.2	123.89–123.89	8.14–12.69	6
Almehaideb et al. (2001) from Aghamiri et al. (2018)	3.45–10.86	0.05–2.73	0–3.94	37.45–66.43	6.50–10.72	2.81–7.78	1.55–8.43	0.66–5.91	0.57–4.61	4.30–21.30	0.75–0.81	150.0–168.0	65.56–151.67	18.39–42.00	5
Almehaideb et al. (2004)	0.11–0.22	2.90–3.87	0.39–7.28	41.43–47.23	4.86–6.13	4.07–5.31	3.95–4.78	2.85–3.56	2.32–3.09	23.88–32.20		209.4–213.8	121.11–121.11	21.02–27.13	3
Al-Meshari (2004)	0–3.95	0.05–3.78	0–4.99	37.45–72.47	4.57–14.09	2.79–8.79	2.00–8.43	1.51–5.91	1.28–4.61	11.45–24.68	0.80–0.87	168.0–257.6	37.78–157.22	15.12–62.90	22
Avaullée et al. (2001)	0–1.25	0.77–8.13	0–0.18	32.36–50.01	5.48–9.79	4.20–7.35	3.62–6.53	2.45–5.30	2.45–5.42	17.54–39.79	0.81–0.86	188.9–332.2	104.40–146.10	15.19–27.58	5
Avaullee et al. (1997)	0.32–0.32	2.80–2.80	1.49–1.49	45.30–45.30	9.11–9.11	5.50–5.50	4.13–4.13	3.06–3.06	2.38–2.38	25.91–25.91	0.85–0.85	220.5–220.5	26.70–121.10	21.24–27.50	7
Coats and Smart (1986)	0.11–1.64	0.08–60.31	0–0.04	7.05–57.49	1.57–13.45	2.46–10.48	1.66–8.40	1.60–5.23	1.51–5.46	12.20–48.24	0.81–0.90	143.0–252.0	55.00–121.11	11.68–30.76	7
Danesh et al. (1992)	0	0	0	36.15–74.18	5.32–12.17	4.67–8.05	2.58–5.81	0.97–4.79	1.56–5.24	10.72–27.79	0.77–0.77	158.0–191.0	100–100	15.43–32.78	4
Dansh from Elsharkawy (2003)	0–0.90	0–3.55	0	36.47–57.53	5.48–10.16	3.70–6.95	2.35–5.37	1.60–2.85	1.33–4.33	19.11–36.12	0.81–0.85	203.0–265.0	90.56–104.44	18.07–34.93	4
Drohm et al. (1988)	0.24	0.27	0	66.83	8.28	5.15	3.31	2.04	1.85	12.03	0.80	182.0	101.67	33.17	1
El-Banbi et al. (2006)	0–1.67	0.10–2.40	0	55.59–72.47	4.57–9.21	2.79–5.89	2.00–4.17	1.51–2.97	1.38–1.97	14.80–19.02			87.78–126.67	31.21–62.56	5
Elsharkawy (2003)	0–0.79	0.07–5.01	0–2.67	5.82–48.79	0.84–11.07	0.43–9.23	1.14–6.07	1.50–4.88	0.99–4.92	24.80–83.20	0.85–0.94	134.0–324.0	54.44–117.22	2.16–25.03	58
Firoozabadi and Katz (1988)	0.03–0.12	2.02–2.98	0	51.53–66.87	6.86–8.07	3.96–5.04	2.55–2.87	1.86–1.89	1.38–1.40	13.40–27.17	0.89–0.89	164.7–217.0	22.78–82.30	31.65–40.68	2
Hoffman et al. (1953)	0	0	0	52.00–52.00	3.81–3.81	2.37–2.37	1.72–1.72	1.20–1.20	2.06–2.06	36.84–36.84	0.84–0.84	199.0–199.0	93.33–93.89	26.40–26.48	3
Hong (1982)	0–1.02	0.01–0.40	0	31.00–54.62	10.41–11.47	7.33–11.87	4.01–7.32	1.96–4.41	1.42–2.55	17.77–32.43	0.74–0.81	199.0–218.0	54.44–73.33	11.17–26.90	2
Jacopy and Berry (1958)	1.67	2.18	0	60.51	7.52	4.74	4.12	2.97	0	16.29	0.789	181.0	118.89	33.26	1
Jamaluddin et al. (2001)	0.48–0.80	0.05–0.92	0	43.43–51.02	8.09–11.02	6.02–6.55	3.97–4.49	3.21–3.53	2.67–2.70	24.17–26.88	0.87–0.88	228.1–368.9	88.00–116.00	22.21–29.37	8
Jamaluddin et al. (2002)	0.49	11.37	3.22	27.36	9.4	6.7	3.98	3.2	2.49	31.79	0.877	248.3	83.20–141.10	17.24–21.10	4
Jaubert and Neau (2002)	0.497	2.13	0	61.887	9.35	5.792	2.865	1.857	2.316	13.307	0.83	213.7	127.90	37.4	1
Jaubert et al. (1995)	0.07–0.45	0–5.40	0–1.40	0.64–59.95	0.56–12.72	1.44–6.84	1.78–6.27	1.44–5.72	1.59–5.34	20.21–84.41	0.82–0.91	211.2–290.1	65.00–132.00	0.55–36.63	10
Jaubert et al. (2002a, 2002b)	0–1.25	0.77–3.60	0–2.32	22.92–54.26	5.48–9.74	4.20–7.37	3.21–6.81	1.95–5.85	1.53–4.84	21.27–45.80	0.82–0.87	200.0–247.6	98.90–121.10	9.69–32.02	13
Jhaveri and Youngren (1988)	0–0	0–9.11	0	45.58–60.88	5.11–7.38	3.03–5.03	2.18–2.78	1.92–1.96	1.54–1.84	20.13–31.53	0.84–0.89	191.0–270.0	87.78–87.78	26.48–34.48	2
Kokal et al. (2003)	0.18	5.21	1.35	25.67	9.19		7.29	8.8	3.59	38.72	0.873	204.9	99.00	13.1	1

(*continued on next page*)

Table 1 (*continued*)

Reference	N_2 (mol%)	CO_2 (mol%)	H_2S (mol%)	C_1 (mol%)	C_2 (mol%)	C_3 (mol%)	C_4 (mol%)	C_5 (mol%)	C_6 (mol%)	C_{7+} (mol%)	SG_{7+}	MW_{7+} (g/mol)	T (°C)	P_b (MPa)	N
Krejbjerg and Pedersen (2006)	0–0.49	0.31–1.44	0	18.72–44.01	0.14–3.84	0.03–1.12	0.02–1.33	0.28–1.04	0.41–1.04	46.84–78.96	0.89–1.01	244.7–524.5	52.00–74.00	7.15–22.72	2
Leibovici et al. (1993)	0.3706	0.7512	0	56.309	107	4.8672	2.4814	1.9859	2.1772	21.0499		214.2	145.56	37.38	1
Li et al. (1985)	1.67	1.38	0	26.68	9.25	10.18	6.4	4.03	0	40.41	0.855	217.0	98.89	13.48	1
McCain (1990)	0.16	0.91	0	36.47	9.67	6.95	5.37	2.85	4.44	33.29	0.848	215.2	104.44	18.17	1
Moharam and Fahim (1995)	0.17–0.77	0.34–3.69	0–3.68	12.59–21.55	6.05–8.60	6.51–8.00	4.26–6.77	4.18–5.87	1.14–6.37	43.41–62.18	0.86–0.89	230.0–275.0	87.78–115.00	6.21–10.97	7
Neau et al. (1993)	0.39–1.81	0.23–3.24	0	45.82–63.00	5.17–10.83	3.46–7.12	2.27–4.25	1.66–3.13	1.27–2.48	12.90–35.56	0.80–0.87	185.6–243.5	85.00–132.50	24.57–39.80	14
Pedersen (2007)	0.39–0.59	0.30–1.01	0	40.20–45.30	3.90–7.61	1.39–7.95	1.44–5.27	1.10–3.54	1.02–2.84	31.56–44.30	0.84–0.89	211.2–253.9	73.00–97.80	19.97–24.04	3
Pedersen et al. (1985)	0.34	0.84	0	49.23	6.32	4.46	3.04	2.26	2.06	31.45	0.865	230.3	93.30	27.45	1
Pedersen et al. (1989)	0.40–0.58	1.00–3.55	0	45.34–53.89	4.20–8.57	0.89–6.05	1.08–3.49	0.94–2.05	1.01–1.45	20.66–45.08	0.85–0.89	203.7–258.1	71.60–141.00	23.90–34.03	3
Pedersen et al. (1992)	0.69	0.12	0	47.06	5.69	4.39	3.37	2.57	2.26	33.85	0.846	211.5	72.80	23.70	1
Pedersen from Elsharkawy (2003)	0.33–0.90	0.16–3.55	0	34.93–50.50	3.36–7.74	0.89–8.20	0.95–5.48	0.40–3.80	0.72–3.04	28.00–57.73	0.82–0.92	210.0–291.0	68.89–114.44	15.91–27.46	9
Pedersen et al. (1988)	0.31	0.69	0	47.69	6.64	4.59	2.59	1.16	1.69	34.64	0.869	234.00	111.11	26.21	1
Regueira et al. (2020)	1.41	0.14	0	49.3	9.78	4.67	1.94	3.18	1.82	27.76	0.808	189.4	24.91–199.89	20.92–26.34	19
Remolina and Parra (2006)	1.28–1.58	1.39–5.84	0	46.78–74.18	5.32–9.65	4.10–8.75	2.58–5.89	0.97–4.57	2.29–6.22	9.49–24.20	0.77–0.84	142.7–183.0	55.44–99.87	20.60–32.80	5
Riemens et al. (1988)	0.71	3.84	1.17	59.49	5.55	4.06	3.06	1.58	1.27	19.27	0.78	297.0	70	47.45	1
Wu and Rosenegger (1999)	0.03–1.39	0.01–8.39	0–1.41	5.63–53.19	1.11–11.69	1.58–9.60	3.50–7.87	1.86–6.65	1.88–6.65	18.42–72.86	0.81–0.96	176.0–261.0	53.33–156.67	2.39–28.66	25
Stenby et al. (1996).	0.403	1	0	45.396	4.202	0.887	1.079	0.941	1.011	45.08		250.5	71.11	29.8	1
Vogel and Yarborough (1980)	0.65	0.02	0	45.02	12.45	8.93	6.03	3.02	1.44	22.44	0.81	184.0	60	20.70	1
Wang and Gmehling (1999)	0.26–0.34	0.20–0.84	0	40.87–49.23	1.63–9.95	1.18–8.35	1.25–6.42	0.86–2.49	0.59–2.06	30.22–45.38	0.82–0.87	213.0–230.3	65.05–93.35	17.37–27.45	7
Williams et al. (1980)	0.25	0.24	0	40.91	10.38	9.01	5.13	3.28	2.21	28.58	0.80	182.0	148.89	20.99	1
Yang et al. (1997)	3.912	0.75	0	70.203	9.22	2.759	1.643	0.824	0.816	9.873	0.803	192.8	40.35–98.45	45.02–46.68	7

data covers a wide range of oil composition from heavy oil to volatile oil with low content of non-hydrocarbon gas. The P_h of crude oil ranges between 0.55 and 62.90 MPa and the saturation temperatures T_h (gas phase homogenization into liquid phase) are between 22.78 °C and 199.89 °C, thus covering the typical ranges of P_h and T_h of oil inclusions in sedimentary basins. The natural gas data primarily consists of gas condensates with minor wet gasses with a variety of non-hydrocarbon gas content. For example, the molar content of N_2, CO_2 and H_2S is as high as 43.22 mol%, 91.92 mol% and 51.37 mol%, respectively. The P_h of gas condensate and wet gas ranges between 4.06 MPa and 81.59 MPa and the dew point temperatures T_h (liquid phase homogenization into gas phase) are between −30 °C and 200 °C, which covers nearly all the possible ranges of P_h and T_h of gas condensate and wet gas inclusions in sedimentary basins. In addition, these collected hydrocarbon fluids from global sedimentary basins are generated from various hydrocarbon source rocks with kerogen types from Type I to Type III, therefore, these hydrocarbon fluids can be regarded as the typical representations of HFIs and then are used to establish the standard fluids for extrapolating the new empirical equations for composition and *P-T* trapping condition prediction of HFIs in this study.

2.3. Thermodynamic modeling of HFI

To obtain accurate P_h, F_v and isochore calculations of HFI the saturation pressure and molar volume of gas and liquid phases should be calculated accurately as a first step. Here we follow the same calculation procedures as Ping et al. (2013b). In short, the C_{7+} composition of each hydrocarbon fluid was first split into C_7 to C_{45+} using the method of Ahmed et al. (1985), with the critical temperature and pressure and acentric factor of extended composition (C_7–C_{45+}) calculated by Cavett (1962) and Riazi and Al-Sahhaf (1996), respectively. The extended composition hydrocarbon fluid compositions were then lumped into six group including C_7, C_8, C_9, C_{10}, C_{n1} ($C_{11\text{-}25}$) and C_{n2} (C_{26+}) which is the same as the model with the α-β composition model (Thiéry et al., 2000, 2002). The calculated saturation pressures were matched to the experimental values by tuning the MW and SG of C_{7+} composition to slightly change the fluid composition based on the experimental error of approximately ± (5–20%) for molecular weight measurement of C_{7+} composition (Thomassen et al., 1987; Zurita et al., 2002; Al-Meshari et al., 2007a). The final adjusted composition and MW and SG of C_{7+} are regarded as the standard composition for HFI. Furthermore, a total of 2494 experimental relative volume data from 98 crude oil and gas condensate samples (Table 3) was used to calibrate the molar volume calculations of gas and liquid phases using a volume translation method based on the final adjusted fluid composition (Jhaveri and Youngren, 1988). The Peng and Robinson EoS (PR-EoS) (Peng and Robinson, 1976) was used to perform the *PVT* phase equilibrium calculations and the binary interactions parameters (BIPs) between the hydrocarbon were set to zero for simplification, while the BIPs were nonzero for the hydrocarbon to non-hydrocarbon interactions based on Zurita et al. (2002). After matching the saturation pressure and calibrating molar volume of gas and liquid phases of hydrocarbon fluids, the accuracy of F_v calculation of HFI has been greatly improved as shown by Ping et al. (2013b) (see Figs. 3 and 4 therein). Finally, a substantial database with hydrocarbon fluid compositions and calculated F_v and P_t values with varying T_t was compiled for the development of new models for *P-T* trapping condition reconstruction of HFI.

3. Results and discussion

3.1. Composition prediction of HFI

The C_{7+} composition in reservoir fluid usually correlates well with gas oil ratio which is defined as the ratio of the respective volumes of liberated gas and residual oil at standard temperature and pressure (STP) and therefore it can also be used as an indicator of the reservoir fluid type (Danesh, 1998; Marruffo et al., 2002). Although the F_v is measured under laboratory conditions with unknown internal pressure in fluid inclusions, the gas oil ratio of reservoir fluid is generally correlated to the F_v of HFI and it is expected that there is a good relationship between the F_v and molar percentage of C_{7+} composition (x_{7+}) for HFI (Ping et al., 2011). Ping et al. (2013b) calculated the F_v under different T_h for 160 crude oils with x_{7+} ranging from 13% to 84% and found that the x_{7+} correlates well with the F_v for the same T_h. Although Ping et al. (2013b) established the correlation between the F_v and x_{7+} of HFI for the first time, two problems limit its wide application including the relatively small amounts of data and absence of gas condensate fluids. Therefore, the correlation is not appliable for HFI which homogenize into the gas phase.

In this study we extend the crude oil samples from previous 160 to 292 reservoir fluid (Table 1) and integrate abundant gas condensate fluid (Table 2). Fig. 2 shows that the x_{7+} is strongly correlated to the F_v under the same T_h from crude oil to gas condensate fluids. It is interesting that there are three types of variation patterns between the F_v and x_{7+} separating by 20% and 12.5% of C_{7+} composition. Usually, the petroleum type can be divided into black oil (>20%), volatile oil (12.5–20%) and gas condensate (<12.5%) based on the x_{7+} (Danesh, 1998). It clear that the relationship between the F_v and x_{7+} is strongly controlled by the type of fluid. The F_v increases relatively slowly with decreasing of x_{7+} for black oils while the F_v increases faster for volatile oil at the same T_h. For gas condensates F_v increases rapidly for decreasing x_{7+} (Fig. 2). Furthermore, with increase of F_v for the gas condensate, the effect of T_h on the F_v is relatively weak especially for the F_v > 50–60%. It indicates that the F_v is the most important factor for determining the x_{7+} of gas condensate inclusion which homogenizes liquid phase into gas phase. In contrast, the x_{7+} of oil inclusion is intensely controlled by the T_h. It means that the T_h may be not important to determine the x_{7+} for gas condensate fluid.

A mathematical relationship between x_{7+} and F_v and T_h has been obtained based on multivariate regression analysis (Eq. (1)) for T_h from 30 °C to 170 °C:

$$x_{7+} = a e^{-\frac{1}{2}\left[\left(\frac{\ln T_h - b}{c}\right)^2 + \left(\frac{\ln F_v - d}{e}\right)^2\right]} \quad (20\% \le x_{7+} < 85\%) \tag{1}$$

where a, b, c, d and e are the coefficients given in Table 4. The coefficient of determination (R^2) for Eq. (1) is as high as 0.98. Eq. (1) can give a very good prediction of x_{7+} with average absolute deviation (AAD) of ~8.3% if the x_{7+} is high than ~20%. However, we found the prediction error of x_{7+} is relatively big with AAD of ~79% if the x_{7+} is lower than ~20%, and the absolute deviation (AD) rapidly increases with decrease of x_{7+} for x_{7+} <3% as shown in Fig. 3 and the maximal AD of predicted x_{7+} can exceed 2000%. To improve the prediction accuracy of the HFI with x_{7+} <20% we obtained another equation (Eq. (2)) by refitting the data with x_{7+} <20%:

$$x_{7+} = \frac{a + bT_h + cF_v}{1 + dT_h + eF_v} \quad (x_{7+} < 20\%) \tag{2}$$

where the coefficients a, b, c, d and e are shown in Table 4. Fig. 3 shows the predictive accuracy for x_{7+} <20% using Eq. (2) has been greatly improved and the AAD is as low as ~31% compared with the 79% using Eq. (1). Eq. (2) gives a better prediction accuracy with AAD of 9.7% and 17.8% for x_{7+} ranging from 12.5 to 20% and 1.5–12.5%, respectively (Table 5). Please note that the HFI with x_{7+} <1.5% is nearly pure gas phase (>99%) under room temperature and thus it is difficult to measure the T_h and F_v. Therefore, even if the predictive accuracy of x_{7+} for these HFI is very low, but it does not affect the application of Eq. (2) to obtain the x_{7+} of gas condensate inclusions.

The x_{7+} is primarily controlled by F_v and T_h of HFI based on this study and previous studies (Ping et al., 2011, 2013b), which indicates that petroleum fluid type can be directly determined if the T_h and F_v of

Table 2
The range of experimental molar composition (%), temperature, and dew point pressure of gas condensate used in this study. SG_{7+}: specific gravity of C_{7+} composition; MW_{7+}: molecular weight of C_{7+} composition (g/mol); *T*: temperature which is equivalent to homogenization temperature (T_h); P_d: dew point pressure which is equivalent to homogenization pressure (P_h); N: number.

Reference	N_2 (mol%)	CO_2 (mol%)	H_2S (mol %)	C_1 (mol%)	C_2 (mol%)	C_3 (mol%)	C_4 (mol%)	C_5 (mol%)	C_6 (mol %)	C_{7+} (mol%)	SG_{7+}	MW_{7+} (g/mol)	*T* (°C)	P_d (MPa)	N
Akpabio et al. (2014)	0.10	0.62	0	80.99	6.64	3.41	1.87	0.88	0.85	4.64	0.83	163.30	103.89	47.10	1
Alarouj et al. (2020)	0.17–1.12	0.36–7.44	0–0	69.05–87.10	6.36–10.85	2.02–6.22	1.09–4.41	0.48–2.96	0.46–4.81	1.23–8.32	0.76–0.77	118.61–147.55	80–154.00	13.90–42.90	6
Almehaideb et al. (2001) from Aghamiri et al. (2018)	0.14–10.86	0.19–4.35	0–3.94	50.47–69.76	4.49–11.56	2.67–7.62	1.55–5.00	0.66–2.60	0.57–2.03	4.30–20.53	0.75–0.85	149.96–250	65.56–152.78	27.45–42.75	15
Almehaideb et al. (2004)	0.27	4.35	2.35	73.10	6.00	3.48	2.57	1.65	1.21	5.08		140	121.11	27.57	1
Al-Meshari et al. (2007a, 2007b)	2.94–7.21	0.51–2.10	0–0.40	68.32–72.08	7.75–10.22	3.97–4.09	2.12–2.49	1.00–1.37	0.71–1.03	4.74–6.95	0	128.00–131.00	120–131.11	38.33–43.11	2
Al-Meshari (2004)	0.11–10.86	0.01–4.35	0–3.94	57.71–72.09	4.49–10.72	2.67–6.23	1.55–4.07	0.66–1.96	0.57–2.03	4.30–12.39	0.79–0.83	145.19–173.00	109.44–151.67	33.94–42.85	10
Arabloo and Rafiee-Taghanaki (2014)	0.34-0.12	1.62-2.45	0-29.1	41.93-70.64	3.9-11.72	2.24-5.46	2.6-3.86	1.36-1.75	0.9-1.75	5.88-13.05	0.80-0.81	153-180	87.22-160.00	27.64-38.26	4
Assareh et al. (2011)	1.48	0.70	0	94.02	1.40	0.45	0.48	0.31	0.21	0.96	0.82	137.73	118.89	23.44	1
Bonyadi and Esmaeilzadeh (2007)	0–5.67	0–2.44	0	45.74–91.35	3.49–13.90	1.40–7.59	0.82–6.38	0.34–4.31	0–5.92	1.34–10.66	0.77–0.80	129.81–177.90	32.22–162.78	20.86–47.04	17
Coats (1985)	5.62–5.67	2.01–2.26	0	45.74–46.79	11.47–12.65	5.87–7.59	6.04–6.38	3.92–4.31	4.78–5.92	10.66–12.32	0.80–0.80	148.00–148.00	162.78–162.78	20.86–21.48	2
Coats and Smart (1986)	0–1.14	0.69–3.50	0–18.19	57.62–70.64	7.39–13.55	3.02–7.61	2.31–4.03	1.29–2.41	0.90–5.54	5.88–11.45	0.77–0.81	117.00–193.00	87.78–130.56	30.68–33.38	3
Donohoe and Buchanan (1981)	0.37–0.46	0.57–0.61	0	59.39–68.64	13.78–13.90	6.89–7.58	3.32–4.07	1.56–2.15	1.14–1.80	3.48–10.29	0.78–0.80	152.30–177.10	89.85–90	23.53–30.16	6
El-Banbi et al. (2006)	0.11–1.62	0.01–6.98	0	59.96–81.23	5.54–14.10	2.66–8.37	1.68–4.93	0.99–2.99	0.83–2.38	6.39–12.69			85.56–155.56	27.58–79.12	8
Elsharkawy (2002b)	0.15–0.87	0.18–3.47	0	64.04–86.57	3.55–10.57	1.44–5.75	0.89–3.72	0.46–4.36	0.35–3.08	2.63–11.18	0.73–0.85	106.00–253.00	15.56–148.89	18.28–81.57	5
Elsharkawy (2002c)	0–10.19	0.17–63.52	0–51.37	19.37–86.16	0.24–11.65	0.07–4.18	0.05–2.81	0.03–1.72	0.02–1.24	0.04–9.91	0.70–0.85	103.00–253.00	48.89–162.78	16.18–81.56	15
Elsharkawy (2003)	0–11.71	0–8.64	0	59.80–95.22	1.62–14.15	0.35–6.89	0.18–4.64	0.08–4.36	0.06–3.08	0.39–11.18	0.72–0.85	106.00–253.00	4.44–169.44	18.28–81.59	14
Firoozabadi et al. (1978)	0.08–0.08	2.44–2.44	0	82.10–82.10	5.78–5.78	2.87–2.87	1.79–1.79	1.12–1.12	0.72–0.72	3.10–3.10	0.77–0.77	132.00–132.00	82.45–82.50	28.10–28.10	3
Folsta et al. (2010)	0.22–4.14	0.19–7.81	0	71.05–97.35	0.49–10.57	0.18–4.82	0.21–2.27	0.10–0.98	0.05–0.55	0.20–1.95	0.77–0.81	128.25–160.15	58.00–100.80	25.00–36.54	4
Guo et al. (2020)	0.57–4.17	0.72–4.22	0	75.55–76.73	2.92–8.80	1.88–3.86	1.12–1.45	0.70–0.75	0.56–1.10	5.23–8.76	0.80–0.81	159.24–194.74	129.00–152.10	42.80–49.89	3
Haghtalab et al. (2011)	0.34–0.75	2.17–3.91	0	70.20–70.64	9.22–10.76	2.76–4.94	1.64–3.02	0.82–1.35	0.82–0.90	5.88–9.87	0.80–0.81	153.00–192.80	117.50–135.70	33.47–46.07	2
Hassan et al. (2018)	3.35	1.76	0.53	83.27	5.16	1.91	1.11	0.56	0.39	1.98	0.77	138.70	104.44	35.40	1
Hoffman et al. (1953)	0	0	0	91.35	4.03	1.53	0.82	0.34	0.39	1.54	0.79	141.10	93.89	26.35	1
Hou et al. (2016)	0.64	5.23	0	57.07	11.73	6.22	2.83	2.29	2.58	11.41	0.75	114.40	132.40	24.48	1
Hou et al. (2020)	0.96–1.28	24.01–51.61	0	35.79–54.78	3.00–4.70	2.11–3.25	1.37–2.19	0.70–1.26	0.29–0.68	4.17–7.84	0.79–0.81	147.23–157.60	113.60–113.60	29.77–31.46	3
Huang et al. (1985)	4.61–5.62	2.01–3.24	0	40.92–46.87	10.86–12.65	5.87–6.86	6.04–6.30	3.53–3.92	2.92–4.78	10.66–16.81	0.79–0.80	132.00–148.00			5
Ibeh and Chubueze (2016)	0.10	0.62	0	80.99	6.64	3.41	1.87	0.88	0.85	4.64			103.94	47.10	1
Imo-Jack (2010)	0.34	1.24	0	79.67	5.47	3.96	2.62	1.42	1.13	4.15	0.77	130	109.44	28.34	1
Jaubert et al. (2000)	0.32–3.71	1.78–2.91	0–1.41	76.62–82.83	4.38–7.40	1.37–3.48	0.94–1.75	0.52–1.07	0.37–0.94	1.55–6.49	0.79–0.81	146.28–170.91	95.00–125.00	36.00–51.00	5
Jia and Wu (2017)	5.58	0.59	0	70.53	9.31		1.42		2.49	10.08			136.50	52.30	1
Joiner and Long (1978)	0.20–0.81	0.20–0.81	0.20–0.81	68.89–89.91	3.70–13.78	1.59–5.84	1.01–2.95	0.64–1.72	0.33–1.35	1.00–7.49			60–131.67	16.82–47.62	12
Kaydani et al. (2016)	0.15–11.71	0.06–8.64	0–0.75	59.80–86.57	1.62–14.15	0.35–6.89	0.18–3.92	0.08–4.36	0.06–3.08	0.39–11.18	0.73–0.85	106.00–253.00	15.56–169.44	18.28–81.56	12
Khodapanah and Tabatabaei-Nejad(2014)	0.10–3.32	1.43–4.00	0–2.69	79.85–82.78	5.24–8.40	1.96–3.19	1.15–1.46	0.56–0.82	0.39–0.57	1.91–3.88			76.67–133.30	23.22–38.99	3
Khoshnamvand et al. (2017)	0.08	2.44	0	82.10	5.78	2.87	3.43	1.12	0.72	3.10	0.77	132.00	82.50	28.10	1
Kilgren (1966)	0.19	1.02	0	86.73	2.48	1.27	1.08	0.34	0.19	6.70	0.88	295.00	127.00	85.80	1
Lagache et al. (2004)	0	0.21	0	80.74	4.90	4.77	3.23	1.89	1.85	2.41			189.85	33.00	1
Leibovici et al. (1993)	0.32	1.95	0	76.15	7.74	3.62	1.89	1.12	1.19	6.02		187.50	30.72–150.17	54.13–74.61	5
Liu et al. (2013)	0.52–0.84	0.44–0.75	0	95.79–96.00	2.10–2.31	0.20–0.21	0.11–0.13	0.04–0.05	0.03–0.04	0.21–0.23	0.80–0.81	151.99–156.08	74.55–146.05	33.24–43.02	8
Louli et al. (2012) from Aghamiri et al. (2018)	0.08–5.56	0.44–2.44	0	82.10–85.48	3.50–5.78	1.46–2.87	0.94–1.79	0.50–1.12	0–0.72	2.10–3.10	0.77–0.79	129.81–143.60	32.22–113.33	28.11–41.48	12
Al-Mahroos and Tjoa (1985)	11.71–11.71	6.50–6.50	0.05–0.05	79.06–79.06	1.62–1.62	0.35–0.35	0.18–0.18	0.08–0.08	0.06–0.06	0.39–0.39	0.80–0.80	161.87–161.87	32.20–169.40	22.96–46.28	4
Majidi et al. (2014)	0–43.22	0–91.92	0–29.86	3.49–96.68	0.37–12.88	0.18–8.58	0.22–20.30	0.06–2.21	0.05–1.52	0.19–10.01	0.76–0.87	126.00–235.00	53.89–142.22	9.69–74.39	20
Maleki et al. (2012) from Aghamiri et al. (2018)	0.34–0.75	2.17–3.91	0	70.20–70.64	9.22–10.76	2.76–4.94	1.64–3.02	0.82–1.35	0.82–0.90	5.88–9.87	0.80–0.81	153.00–192.80	135.55–177.15	33.49–45.33	4
Mazloom et al. (2004) from Aghamiri et al. (2018)	0.52–0.84	0.44–0.75	0	95.79–96.00	2.10–2.31	0.20–0.21	0.11–0.13	0.04–0.05	0.03–0.04	0.21–0.23	0.80–0.81	151.99–156.08	74.55–146.05	33.26–43.04	8
Mehrabian and Crespo (2011)	2.91–3.49	1.99–2.29	0.13–0.34	81.42–82.86	5.01–5.39	1.79–2.07	1.13–1.30	0.66–0.88	0.39–0.88	2.64–3.09			97.28–105.00	34.13–36.75	5
Nasrifar et al. (2005)	0–0.87	0–8.64	0	64.04–91.35	3.76–13.90	1.44–6.89	0.82–3.72	0.34–4.36	0.39–3.08	1.54–11.18	0.73–0.83	106.00–200	15.70–171.00	18.28–60.33	7

(*continued on next page*)

Table 2 (*continued*)

Reference	N_2 (mol%)	CO_2 (mol%)	H_2S (mol %)	C_1 (mol%)	C_2 (mol%)	C_3 (mol%)	C_4 (mol%)	C_5 (mol%)	C_6 (mol %)	C_{7+} (mol%)	SG_{7+}	MW_{7+} (g/mol)	T (°C)	P_d (MPa)	N
Nemeth and Kennedy (1967)	0–43.22	0–91.92	0–29.86	3.49–96.68	0.37–15.13	0.18–10.90	0.15–8.01	0.06–12.30	0.04–8.71	0.19–13.56	0.73–0.87	106.00–235.00	4.44–160	9.69–74.39	543
Ng and Robinson (1986)	0	0	0	74.13	7.21	4.50	0.87	1.76	2.59	7.10			−17.75–37.85	16.59–23.00	4
Nowroozi et al. (2009) from Aghamiri et al. (2018)	0–0.87	0–8.64	0–0.75	59.80–86.57	3.83–14.15	1.97–6.89	1.21–4.64	0.74–2.70	0.46–1.77	2.92–11.18	0.74–0.83	125.00–200	4.44–159.44	21.34–60.33	9
Nowroozi et al. (2009) from Haji-Savameri et al. (2020)	0–9.36	0–91.40	0–3.94	3.52–95.28	0.10–11.89	0.06–6.34	0.04–3.13	0.02–1.85	0.01–1.44	0.03–10.82	0.74–0.84	104.50–208.07	62.22–145.00	14.72–54.47	59
Pedersen (2007)	0.64	3.53	0	70.78	8.94	5.05	2.53	1.41	0.83	6.29	0.81	165.10	150.50	38.15	1
	0.65–0.65	11.58–11.58	0	85.07–85.07	1.83–1.83	0.48–0.48	0.21–0.21	0.07–0.07	0.03–0.03	0.08–0.08	0.82–0.82	87.04–87.04	−30–8.50	4.06–7.22	4
Pedersen et al. (1985)	0.12–0.64	2.49–9.16	0	68.80–76.43	7.46–8.43	3.12–5.11	1.80–2.26	1.05–1.09	0.63–0.79	3.92–6.70	0.81–0.82	158.83–174.33	129.00–129.00	46.40–46.40	2
Pedersen et al. (1988)	0.71	8.64	0	70.85	8.53	4.95	2.01	0.81	0.46	3.04	0.83	155.30	118.89	39.85	1
Pedersen et al. (1989)	0.60	3.34	0	74.16	7.90	4.15	2.15	1.19	0.81	0.63	0.81	151.06	155.00	38.80	1
Qi et al. (2007)	0.33	2.37	0	79.26	8.81	4.75	2.36	0.87	0.28	0.98			115.00–135.00	42.76–43.55	3
Raffie and Tennyson (2003)	0.05–0.13	0.37–0.78	0	87.71–91.85	3.73–3.87	1.29–1.95	0.58–1.21	0.25–0.55	0.16–0.38	1.58–3.64	0.79–0.80	142.00–159.00			3
Reamer and Sage (1950)	0	0.10	0	95.22	1.68	0.91	0.59	0.27	0.25	0.98	0.72	122.60	104.44	23.06	1
Regueira et al. (2020)	0.10	2.40	0	82.70	6.43	2.34	1.03	0.45	0.35	4.20	0.80	162.40	25.00–200	45.60–69.55	11
Remolina and Parra (2006)	0.31–24.41	0.91–3.67	0	68.70–81.80	3.33–7.80	1.44–3.55	0.70–2.16	0.26–1.32	0.11–1.09	0.14–8.21	0.71–0.82	108.22–184.00	−84.43-137.78	6.70–46.60	3
Sage and Olds (1947)	0	0	0	82.38	4.28	3.51	4.64	1.28	0.99	2.92	0.74	125.00	4.44	21.34	1
Silverman and Hill (1997)	1.92	43.89	2.35	11.62	3.03	4.84	4.45	3.45	2.29	22.16			21.50–44.00	8.71–11.45	3
Sportisse et al. (1997)	0.16–3.71	0.69–3.97	0.26–2.28	64.18–88.86	3.38–9.77	1.18–6.87	0.48–2.82	0.19–1.80	0.02–1.68	0.23–12.41	0.77–0.83	121.68–206.30	30–182.90	17.06–71.50	20
Standing (1979) from Aghamiri et al. (2018)	1.72	0.30	0	79.17	7.48	3.29	1.77	0.91	0.62	4.74	0.77	169.92	120.85	47.06	1
Sun et al. (2012)	0.61–0.85	0.31–0.59	0	87.50–96.68	1.64–7.53	0.22–1.49	0.11–0.61	0.05–0.21	0.02–0.14	0.20–1.31	0.78–0.80	122.78–139.46	30.05–145.45	22.03–46.55	16
Thomas et al. (2006)	0.24	2.01	0	82.36	5.08	3.46	1.74	0.62	0.17	4.30	0.83	172.23	119.00	73.08	1
Vega and Barrufet (2005) from Aghamiri et al. (2018)	0.68–0.98	8.02–8.35	0	67.61–68.74	8.17–8.44	4.70–4.89	2.02–2.32	0.94–1.15	0.59–0.72	5.36–6.87	0.73–0.74	161.72–179.11	120–120	36.11–39.11	7
Vega and Barrufet (2005)	0.25	4.61	0	61.71	9.44	5.14	3.16	1.72	1.27	12.70			140.56	36.70	1
Vogel and Yarborough (1980)	0.20–2.20	0.06–2.12	0	67.50–74.17	9.31–11.27	4.86–5.75	2.80–3.53	0.99–1.48	0.58–1.51	2.00–9.05	0.74–0.80	116.00–162.00	59.85–107.85	20.70–35.90	3
Wang and Gmehling (1999)	0.08–1.94	1.21–2.44	0	65.99–82.10	5.78–10.76	2.87–5.91	0–1.57	0.75–2.69	0.46–1.81	3.10–6.59	0.77–0.81	132.00–153.00	82.55–140.05	23.73–41.94	4
Yan et al. (2001)	2.89–3.11	0.51–0.55	0	70.93–75.57	8.85–9.10	2.78–2.83	1.14–1.20	0.63–0.91	0.46–0.73	6.67–11.15	0.81–0.81	193.50–193.50	29.95–151.95	42.50–58.16	32
Yang et al. (2020)	0	0	0	78.58	8.34	7.96	0.82	0.24	1.24	2.82			110.40	26.30	1
Yang et al. (1997)	3.91	0.75	0	70.20	9.22	2.76	1.64	0.82	0.82	9.87	0.80	192.80	117.75–177.15	42.88–46.07	4
Yushchenko and Brusilovsky (2015)	0.01–0.26	0.14–13.34	0–25.77	52.34–92.08	2.19–7.68	0.98–4.06	0.67–2.25	0.26–0.89	0.19–0.53	1.16–4.99		119.53–185.60	55.45–110	23.02–50.50	3
Zhang et al. (2020)	2.13	1.22	0	65.80	8.51	5.86	9.89	0	0	6.59			93.35	28.00	1

Table 3
The range of experimental molar composition (%), temperature and pressure of crude oil and gas condensate used for relative volume measurement. *T*: temperature; *P*: pressure; N: number of measured relative volume.

Reference	Fluid type	N_2 (mol%)	CO_2 (mol%)	H_2S (mol %)	C_1 (mol%)	C_{7+} (mol%)	*T* (°C)	*P* (MPa)	N
Al-Meshari (2004)	Oil	0–3.95	0.05–3.78	0–4.99	37.45–72.47	11.45–24.68	80–157.22	1.38–96.63	298
Avaullée et al. (2001)	Oil	0–1.252	0.774–8.13	0–0.184	32.357–50.009	17.538–39.791	104.4–146.1	11.15–40.1	58
Bonyadi and Esmaeilzadeh (2007)	Oil	0.72	0.3	0	79.17	5.74	120.85	17.99–49.53	14
Coats and Smart (1986)	Oil	0–1.64	0.08–60.31	0–0.04	7.05–58.32	11.45–48.24	43.3–121.1	1.78–41.37	250
Jaubert et al. (2002a, 2002b)	Oil	0–1.252	0.774–3.601	0–2.32	22.92–54.26	21.27–45.8	26.7–144.7	5–50.05	196
McCain (1990)	Oil	0.16	0.91	0	36.47	33.29	104.44	3.26–34.48	23
Pedersen (2007)	Oil	0.39	0.3	0	40.2	31.95	97.5	5.56–35.14	16
Regueira et al. (2020)	Oil	1.41	0.14	0	49.3	27.76	24.91–200	5.69–53.71	186
Yang et al. (1997)	Oil	3.912	0.75	0	70.203	9.873	40.35–98.45	4.49–46.68	53
Yan et al. (2001)	Oil	2.89–2.96	0.51–0.52	0	70.93–72.46	9.67–11.15	29.95–127.95	6.03–49.58	117
Akpabio et al. (2014)	Gas condensate	0.1	0.62	0	80.99	4.64	103.89	9.59–66.04	17
Al-Meshari (2004)	Gas condensate	0.11–10.86	0.01–4.35	0–3.94	57.71–72.09	4.3–12.39	37.78–151.67	5.62–62.16	448
Bonyadi and Esmaeilzadeh (2007)	Gas condensate	0.72–5.67	0.3–2.26	0	45.74–86.003	1.34–10.66	106.67–162.78	8.02–63.81	59
Coats (1985)	Gas condensate	2.01–2.26	5.62–5.67	0	45.74–46.79	10.66–12.32	162.78	8.03–63.81	38
Coats and Smart (1986)	Gas condensate	0.34–0.42	0.61–2.17	0–0.04	57.49–70.64	5.88–12.2	87.78–130.56	7.17–48.26	45
Guo et al. (2020)	Gas condensate	0.569–4.166	0.722–4.22	0	75.55–76.73	5.232–8.761	129–152.1	6–49.89	22
Hou et al. (2016)	Gas condensate	0.636	5.228	0	57.067	11.411	132.4	7–25.53	13
Imo-Jack (2010)	Gas condensate	0.34	1.24	0	79.67	4.15	109.449	12.62–41.37	17
Kilgren (1966)	Gas condensate	0.19	1.02	0	86.73	6.7	26.67–77.78	6.54–88.35	18
Pedersen et al. (1989)	Gas condensate	0.6	3.34	0	74.16	5.69	155	14.62–59.71	26
Regueira et al. (2020)	Gas condensate	0.1	2.4	0	82.7	4.2	25–200	6.83–73.43	279
Yan et al. (2001)	Gas condensate	2.89–3.11	0.51–0.55	0	70.93–75.57	6.67–11.15	39.35–151.95	5.93–58.16	252
Yang et al. (1997)	Gas condensate	3.912	0.75	0	70.203	9.873	117.75–177.15	4.48–46.07	49

HFI are known (e.g., Bourdet et al., 2008). The T_h can be accurately measured within ±0.1 °C and the F_v measurement of HFI has been reported to an accuracy better than 95% (Pironon et al., 1998). Therefore, the x_{7+} of HFI from heavy oil to gas condensate can be predicted with relatively high accuracy. In order to simply characterize the composition of HFI using Eq. (1) and Eq. (2), we establish a T_h vs. F_v diagram with varying iso-x_{7+} which separates the hydrocarbon fluid into black oil, volatile oil and gas condensate (Fig. 4). Both the petroleum type and x_{7+} of HFI can be directly constrained by Fig. 4 with measured T_h and F_v. To calculate the x_{7+} of HFI we suggest plot the measured T_h and F_v in Fig. 4 firstly and if the data points are within the zone with iso-x_{7+} ≥20% then calculate the x_{7+} using Eq. (1), otherwise, using Eq. (2). In addition, the co-variation of T_h vs. F_v in Fig. 4 is good indicator of multiple petroleum populations (Bourdet et al., 2008; Ping et al., 2012) and can be used to recognize possible post-trapping modifications including stretching and leakage (Bourdet et al., 2008).

Methane molar percentage (x_1) in HFI is another import parameter for determining *PVT* phase behavior and hydrocarbon fluid evolution. However, it is relatively difficult to measure directly. Because of the fluorescence interference conventional Raman spectrum cannot be used to detect the methane in the fluorescent HFI especially the crude oil and gas condensate inclusions (Burruss, 2003). Three-dimensional multimodal coherent anti-Stokes Raman scattering (CARS) microscopy supply the possibility for identifying and mapping methane in the oil inclusions, but quantitative estimation of methane mole fraction cannot be achieved up to now (Burruss et al., 2012). Currently, quantitative FT-IR analysis is the only effective method to directly estimate the methane concentration in petroleum inclusions based on the measurement of CH_2/CH_3 ratio and CH_4/alkane area ratio, while the presence of branched alkanes and CH aromatic groups significantly influence the methane content estimation (Pironon et al., 2001). In fact, the methane content in hydrocarbon fluid is usually inversely proportional to the heavy hydrocarbon content with increasing of thermal maturity due to kerogen cracking in source rocks and oil cracking in reservoirs (Behar et al., 2008; Stainforth, 2009). Therefore, it is likely to obtain an empirical correlation between the x_1 and the x_{7+} in hydrocarbon fluid. In order to limit the effect of non-hydrocarbon gas (N_2, CO_2 and H_2S) we divide our collected crude oil and natural gas samples into two groups 1) samples with relatively high non-hydrocarbon gas content (single gas molar percentage >10%) and 2) samples with relatively low non-hydrocarbon gas content (single gas molar percentage <10%). In addition, several oil samples with abnormal high C_2/C_3 molar content ratio could undergo obvious biodegradation which preferentially consume propane in natural gas (Boreham et al., 2008). As a result, the methane molar content of these oil samples is significantly higher than that of the normal crude oils and therefore these oil samples were eliminated for linear fitting between the x_1 and x_{7+}.

A total of 922 composition data of crude oil and gas condensate fluids was used to obtain the empirical equation (Eq. (3)) between the x_1 and x_{7+} (Fig. 5):

$$x_1 = e^{\left(\frac{a+b\ \ln\ x_{7+}}{1+c\ln\ x_{7+}+d\ln\ x_{7+}^2}\right)} \quad (3)$$

where the coefficients a, b, c and d are shown in Table 4. Please note Eq.

Table 4
The fitting coefficients of empirical equations in this study.

	Eq. 1	Eq. 2	Eq. 3	Eq. 4	Eq. 5	Eq. 6	Eq. 9	Eq. 12	Eq. 13	Eq. 14
a	54606.03198	19.99586	4.48740	90.92996	0.420	0.21124796	10.44896456	0.960895026	0.237632	−8.249468
b	14.60000	−0.0018996	−1.01699	−1.212504	−0.013	0.09416298	−0.04427521	−0.009337081	0.140522	0.123503
c	3.050358	−0.1637082	−0.210896	−0.888273	0.230	−0.89789385	0.45996706	−0.002752781	−0.929211	0.017541
d	−1.964944	−0.0048583	−0.000655458	−1.035100	0.000054	−2.49675529	0.00064377	0.000061035	−2.686313	−0.000578
e	−2.195768	0.0153265		−1.244707	−0.0014	−0.95629988	−0.00328999	0.000020050	−1.072408	0.000017577
f					0.00000025	−5.46566073	−3.6893495E-06	−0.000001135	−5.840817	0.000000971
g					0.000058	127.71771161	3.7381694E-05	0.000000034	1072.734320	−0.000000123
h					0.0037	−828.73639836	−1.0426722E-03	−0.000014442	4676.752367	−0.00020489
i					−0.0000094	0.00654416	1.3792391E-05	0.000000628	0.0059816	0.000000302
j					−0.0000084	−0.00898323	6.8991077E-06	−0.000000917	−0.027326	0.000000193
k						−0.80993511			−8.317518	
l						0.00010840			0.000871	
m						−7.330824E-09			3.42E-09	
n						−13.52773342			−1038.779458	
o						0.05006965			5.498120	
p						−7.752104E-05			−0.009486	
q						1888.122066			60671.392605	

(3) is suitable for the hydrocarbon fluids if the molar percentage of single non-hydrocarbon gas is lower than 10%. Actually, the molar content of non-hydrocarbon gas in crude oil (e.g., x_{7+} >12.5%) is very low. According to our statistics, 98% samples in the collected crude oil samples have molar content of non-hydrocarbon gas lower than 10% and the average value for N_2, CO_2 and H_2S is 0.9%, 1.4% and 0.2%, respectively. Nearly 95% gas condensate fluids have molar content of non-hydrocarbon gas lower than 10%, but for the other 5% samples the molar content of non-hydrocarbon gas is as high as 43% for N_2 (averaging 8%), 92% for CO_2 (averaging 12%) and 53% for H_2S (averaging 11%). Therefore, it is not necessary to consider the content of non-hydrocarbon gas for most of the HFI when predicting the x_1 using Eq. (3) and the AAD of predicted x_1 is ~13.1% and ~6.3% for crude oil and gas condensate, respectively, with an AAD of ~7.9% for all the samples (Table 5). However, if the molar content of single non-hydrocarbon gas is higher than 10%, the predictive error using Eq. (3) could be great. Under this situation the molar content of non-hydrocarbon gas in HFI should be known to obtain a more accurate prediction of x_1 using the fitting Eq. (4) based on 57 crude oil and gas condensate samples:

$$x_1 = a + bx_{N_2} + cx_{CO_2} + dx_{H_2S} + ex_{7+} \ (x_{N_2} > 10\%, or\ x_{CO_2} > 10\%, or\ x_{H_2S} > 10\%) \quad (4)$$

where the coefficients a, b, c, d and e are shown in Table 4. The AAD of predicted x_1 is as low as 14.2%. Please note that gas condensate samples for extrapolating Eq (4) are relatively few and the predicted accuracy of x_1 cannot be adequately evaluated and the result is only for reference. In addition, it is very difficult to obtain the molar content of non-hydrocarbon gas in HFI, and no analytical technique can currently quantitatively measure compositions of all non-hydrocarbon gases in fluid inclusions. In this case, it is best to use the approximate non-hydrocarbon composition data of oil or gas reservoirs.

3.2. Homogenization pressure (P_h) prediction

The homogenization condition (T_h, P_h) connects the trapping condition (T_t, P_t) through the isochores in the *P-T* phase diagram of HFI (Fig. 1). Therefore, P_h is very important for P_t reconstruction. Traditional P_h prediction is primarily based on the iterative calculations to obtain final fluid compositions by inputting T_h, F_v and an assumed initial composition from either a reservoir fluid or an α-β composition model (Aplin et al., 1999; Thiéry et al., 2002). However, the iterative fluid composition is largely dependent upon the selection of initial fluid composition and thus results in great uncertainty in P_h calculations (Ping et al., 2013a). Ping et al. (2011) found that the P_h is primarily determined by the methane molar percentage for crude oil. They developed a mathematical correlation of P_h between T_h and the x_1 based on 160 crude oil samples (Ping et al., 2013b). Compared with the traditional P_h prediction, the Ping et al. (2013b) correlation does not need to iterative calculation to obtain pseudo-composition and thus greatly decreases the unknown parameters for P_h calculation. HFI can be divided into two types 1) HFI homogenizing into liquid phase and 2) HFI homogenizing into gas phase. The former HFI indicates that the hydrocarbon fluid is liquid phase during trapping, including crude oil and parts of gas condensate while the later HFI is homogenizing into gas phase during trapping primarily including gas condensate. In this study we still follow the method of Ping et al. (2013b) and try to establish a new correlation between P_h and T_h and x_1 based on more crude oil and gas condensate samples (Tables 1–2), which extends P_h calculation from crude oil to gas condensate fluids.

As stated in the method section, we firstly create a standard fluid database where their homogenization pressures have been matched and then we calculate P_h for each fluid at T_h ranging from 30 °C to 170 °C with 10 °C interval. Finally, a total of 4511 $T_h \sim x_1 \sim P_h$ data pairs are used to extrapolate the correlation of P_h for HFI which homogenizes into liquid phase. The new P_h calculation equation is shown in Eq. (5):

Table 5
Prediction accuracy of empirical equations in this study. MIN: minimum; MAX: maximum; AD: absolute deviation; AAD: average absolute deviation; P_b: bubble point pressure; P_d: dew point pressure, N: samples number.

	Eq. (1) $x_{7+}>20\%$	Eq. 2 1.5% < x_{7+} < 12.5%	Eq. 2 12.5% < x_{7+} < 20%	Eq. (3) $x_{7+}>12.5\%$	Eq. (3) $x_{7+}<12.5\%$	Eq. 3	Eq. 4	Eq. (5) for measured P_b	Eq. (5) $x_{7+}>12.5\%$	Eq. (5) $x_{7+}<12.5\%$	Eq. 5	Eq. (6) for calculated P_d	Eq. (6) for measured P_d	Eq. (9) $x_{7+}>12.5\%$	Eq. (9) $x_{7+}<12.5\%$	Eq. 9	Eq. 12	Eq. 13	Eq. 14
N	2925	4472	357	232	690	922	57	285	3587	1209	4795	5718	781	3245	1199	4444	1099	5710	1547
MIN AD	0	0.02	0.07	0.03	0.01	0.01	0.02	0	0	0	0	0	0.074	0	0	0	0	0.007	0.02
MAX AD	33.9	231.6	49.6	100.9	43.5	100.9	87.1	83.3	83.3	49.3	83.3	149.6	94.9	52.6	61.4	61.4	30.3	153.3	195.5
AAD	8.3	17.8	9.7	14.3	6.3	8.3	14.2	8.7	7.3	12.7	8.6	18.9	15.8	7.1	12.6	8.6	4.9	19.3	21.6

$$P_h = a + bT_h + cx_1 + dT_h^2 + ex_1^2 + fT_h^3 + gx_1^3 + hx_1T_h + iT_h^2x_1 + jT_hx_1^2 \quad (5)$$

where the coefficients a, b, c, d, e, f, g, h, i and j are listed in Table 4. Eq. (5) is applicable to the HFI with methane molar content ranging from 0.66% to 80.93% and single non-hydrocarbon gas content <10%. Therefore, this equation can not only calculate the P_h of heavy oil and volatile oil, but also the P_h of gas condensate fluid if the inclusion homogenizes into liquid phase. Essentially, all the HFI that homogenize into liquid phase can use Eq. (5) to predict P_h. Eq. (5) can be used to calculate P_h of HFI homogenizing into liquid phase with a wide range of T_h (22–200 °C) and x_1 (0.66–80.9 mol%) and an AAD of 8.6% for a total of 4795 data will be obtained (Table 5). The model (Eq. (5)) has been tested for measured P_h data from 285 crude oils and the AAD of predicted P_h is 8.7% (Table 5), which is better than that from the Ping et al. (2013b) (AAD = 9.5%), Elsharkawy (2003) (AAD = 11.5%) and Jarrahian et al. (2015) (AAD = 34.6%) correlations. Please note that the Elsharkawy (2003) and Jarrahian et al. (2015) models used 10 compositions (N_2, CO_2, H_2S, C_1, C_2, C_3, C_4, C_5, C_6, C_{7+}) together with the SG_{7+} and MW_{7+} of the C_{7+} composition, while our model only needs x_1 and has better predictive accuracy. However, we found that the predictive accuracy of our model slightly depends on the types of hydrocarbon fluid. For crude oil with x_{7+} >12.5% and x_1<62% Eq (5) can obtain a better accuracy (AAD = 7.3%), while the P_h prediction accuracy for gas condensate fluid (x_{7+} <12.5%) an AAD of 12.7% can be obtained (Table 5).

In comparison with the crude oil, the P_h prediction of gas condensate has always been a difficult problem, as it is not only the function of x_1 but also strongly related to other parameters including non-hydrocarbon, C_{2+} composition and physical properties of the C_{7+} composition (Fig. 6). Therefore, more detailed compositions together with SG_{7+} and MW_{7+} are necessary to obtain a better P_h prediction through empirical models (Nemeth and Kennedy, 1967; Elsharkawy, 2002b; Godwin, 2012; Kamari et al., 2016), EoS (Valiollahi et al., 2016; Novak et al., 2018) and artificial neural networks in conjunction with genetic algorithm (Najafi-Marghmaleki et al., 2016; Zhong et al., 2018; Haji-Savameri et al., 2020). In this study, we firstly tried to obtain an acceptable P_h prediction accuracy only using the molar composition of gas condensate like crude oil, while we found that the predictive error of P_h could be very large without the incorporation of other parameters such as SG_{7+} and MW_{7+}. However, it is impossible to directly obtain the SG_{7+} and MW_{7+} of the C_{7+} composition for natural HFI. Here we establish simple linear correlations between x_{7+} and SG_{7+} and MW_{7+} and then the P_h predictive equation was obtained through a nonlinear fitting method based on 13 variables including (N_2, CO_2, H_2S, C_1, C_2, C_3, C_4, C_5, C_6, C_{7+}, SG_{7+} and MW_7, T_h). Although we have collected more than 900 gas condensate data, the measured P_h of these fluids are still too few to represent all the range of P_h with wide variation of T_h. Thus, we matched the measured P_h of the collected samples (see method section and Ping et al. (2013b)) and then calculated the P_h at T_h from 30 °C to 170 °C with 10 °C interval. Finally, a total of 5720 P_h data of gas condensate was used to develop the P_h prediction model in this study. For most of the gas condensate samples, the molar content of single non-hydrocarbon gas is lower than 10% which do not have apparent effect on the P_h prediction. Therefore, the P_h of HFI which homogenizes into gas phase (30 °C < T_h < 170 °C) can be calculated using the following equation:

$$\begin{aligned} P_h = {} & ax_1 + bx_2 + cx_3 + dx_4 + ex_5 + fx_6 + gx_{7+} + hSG_{7+} + i\frac{x_1}{x_{7+}} + jT_h \\ & + kx_{7+}MW_{7+} + l(x_{7+}MW_{7+})^2 + m(x_{7+}MW_{7+})^3 + n\frac{MW_{7+}}{SG_{7+}} \\ & + o\left(\frac{MW_{7+}}{SG_{7+}}\right)^2 + p\left(\frac{MW_{7+}}{SG_{7+}}\right)^3 + q \end{aligned} \quad (6)$$

where the coefficients a, b, c, d, e, f, g, h, i, j, k, l, m, n, o, p and q are

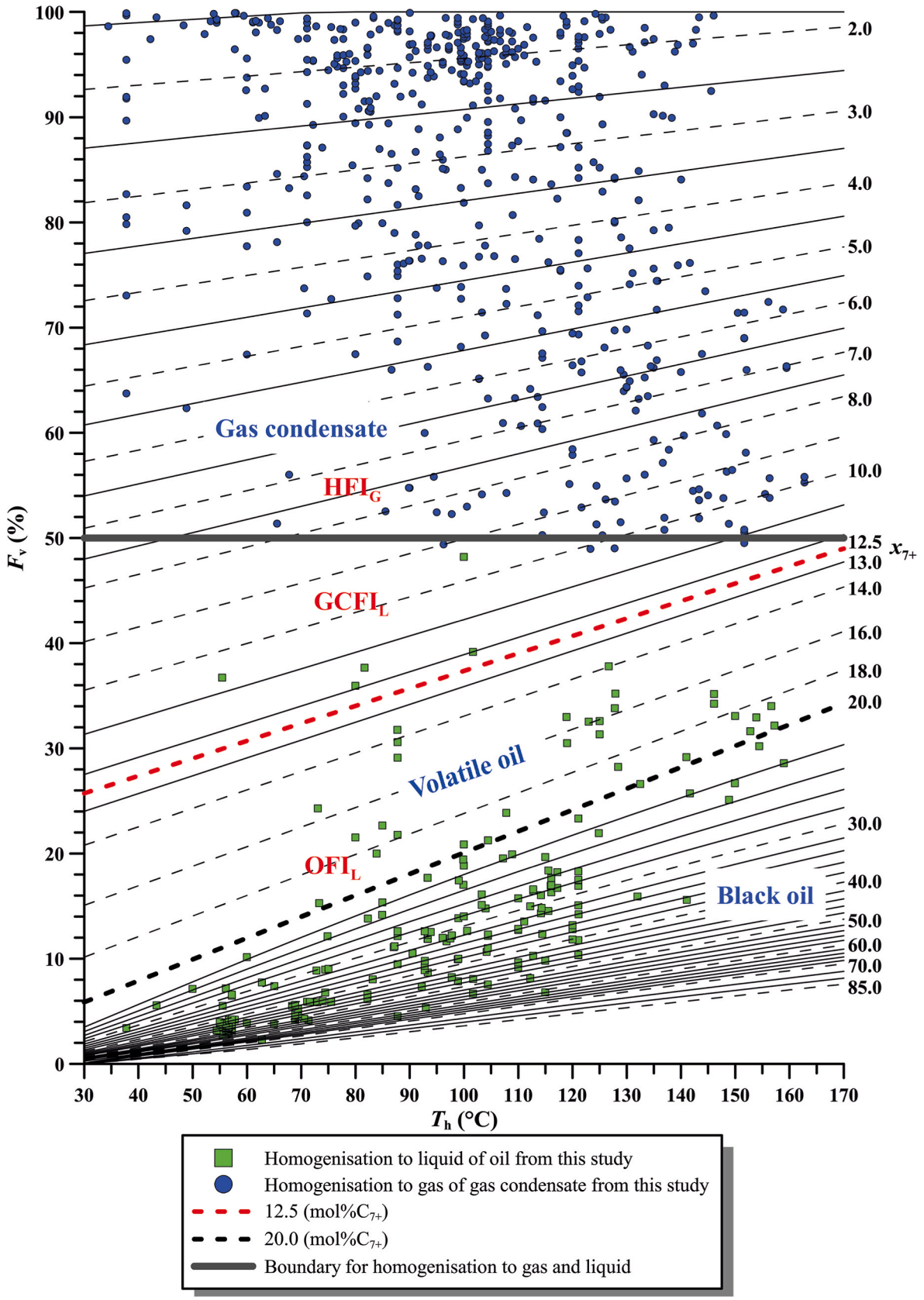

Fig. 4. T_h vs. F_v (calculated at 20 °C) diagram (Bourdet et al., 2008) for varying hydrocarbon fluid compositions which is indicated by the x_{7+}. The F_v is calculated using Eq. (1) and Eq. (2) and the petroleum types are divided into black oil, volatile oil, gas condensate by x_{7+} (Danesh, 1998). OFI$_L$ is oil-bearing fluid inclusion which homogenizes into liquid phase, GCFI$_L$ is gas condensate-bearing fluid inclusion which homogenizes into liquid phase, HFI$_G$ is hydrocarbon fluid inclusion which homogenizes into gas phase. Please note the GCFI$_L$ and HFI$_G$ are separated by the iso-F_v line with approximate 50%. The data points are from collected samples in this study. The dark blue solid circles are from gas condensate samples and the green solid circles are from crude oil samples.

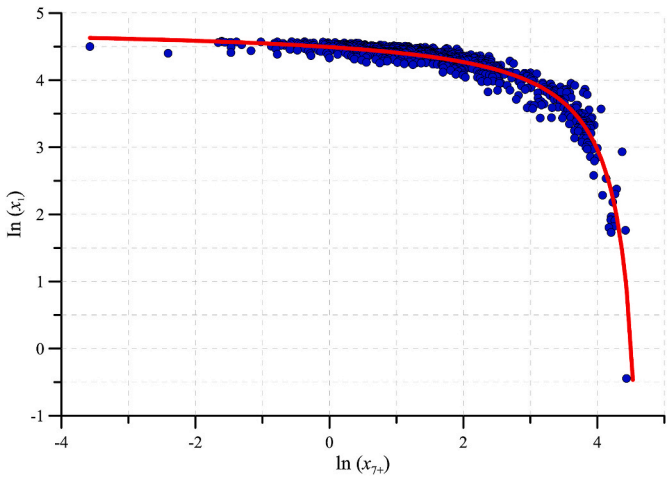

Fig. 5. Relationship between the lnx_1 and lnx_{7+} for measured petroleum compositions.

listed in Table 4. The x_2-x_6 are the molar percentage of C_2–C_6 composition. The SG_{7+} and MW_{7+} are calculated from the following equations:

$$SG_{7+} = 0.0045 * x_{7+} + 0.761 \quad (7)$$

$$MW_{7+} = 6234 * SG_{7+}{}^2 - 8975 * SG_{7+} + 3354 \quad (8)$$

The AAD of Eq. (6) for 5718 data is around 18.9% and the AAD of predicted P_h for 787 measured dew point pressures of gas condensate fluids with molar content of single non-hydrocarbon gas <10% is around 15.8% (Table 5), which is comparable to other empirical models, e.g., Nemeth and Kennedy (1967)'s (AAD = 13.3%) and Elsharkawy (2002)'s (AAD = 15.2%) correlations (Haji-Savameri et al., 2020). Please note other models used the measured SG_{7+} and MW_{7+} while our model calculated them only based on the x_{7+} which can be obtained by T_h and F_v (Eqs. (1) and (2)). Therefore, the developed model (Eq. (6)) in this study can be easily used for fluid inclusion study while others cannot. In addition, we found the new model can also be used to calculate the P_h of gas condensate with high content of non-hydrocarbon gas (>10 mol%) by assuming the molar content of non-hydrocarbon is lower than 10% and an AAD of ~25.9% is obtained for 38 samples. Because of the scarcity of high non-hydrocarbon-content gas condensate samples the P_h

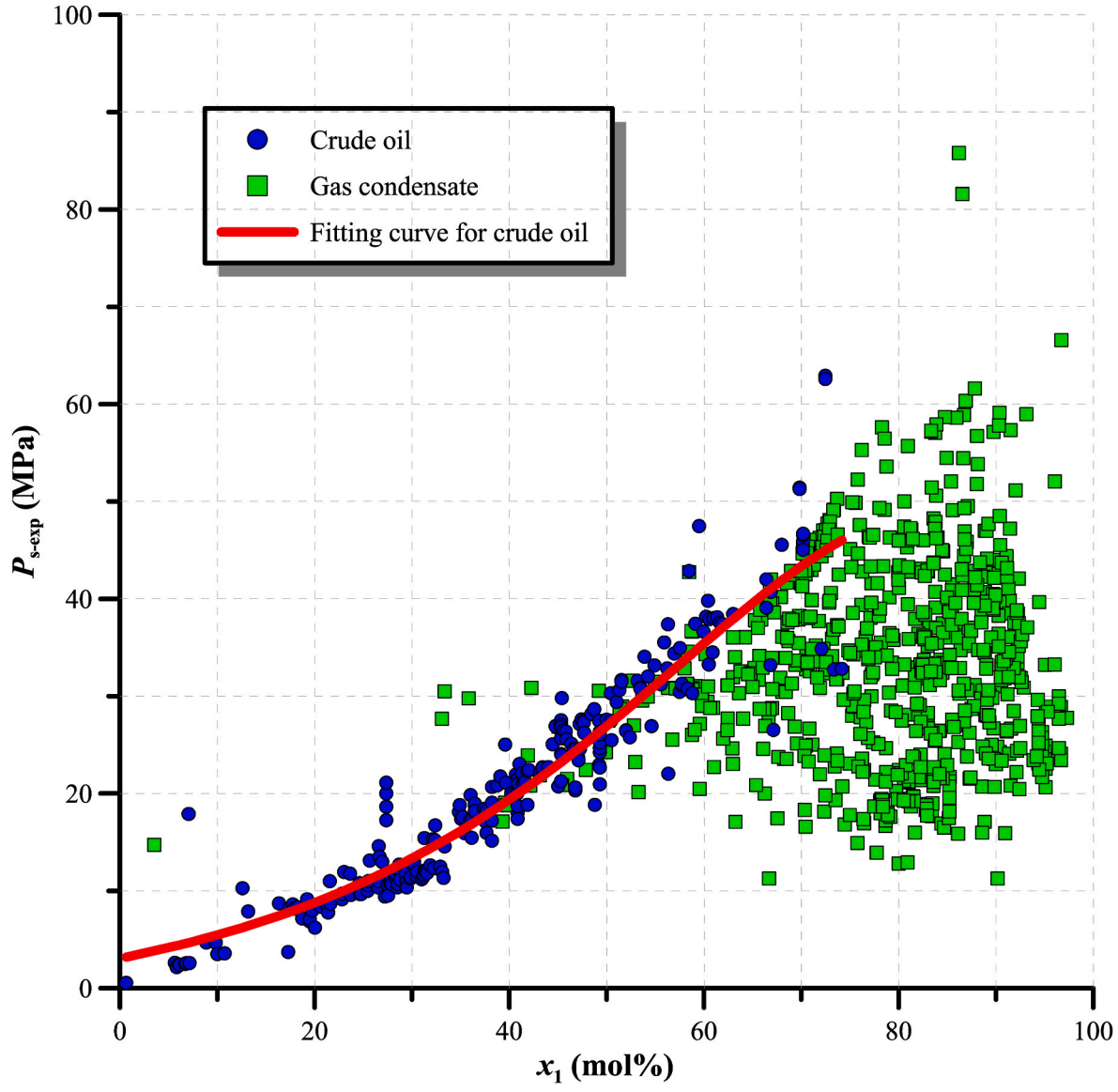

Fig. 6. Relationship between the experimentally measured saturation pressure ($P_{s\text{-}exp}$) and x_1 for crude oil and gas condensate fluids.

prediction equation for this type of fluid is not separately fitted in this study. For most HFIs we can assume that the non-hydrocarbon gas content is lower than 10 mol% and only the molar content of C_1–C_{7+} needs to be known to calculate the P_h of HFIs. Moreover, we calculated the P_h using the PR EoS with the same composition and SG_{7+} and MW_{7+} used in Eq. (6) and an AAD of 21.6% is obtained, indicating the highest P_h prediction accuracy of our new model for fluid inclusion application.

3.3. Trapping pressure predictions

Traditional trapping pressure prediction needs the calculation of isochore using EoS with known detailed fluid composition and P_h ($T = T_h$) of HFI (Aplin et al., 1999; Thiéry et al., 2002), which significantly increase the difficulty for accurate prediction of trapping pressure. As discussed in the previous sections the P_h of HFI homogenizing into liquid phase can be well correlated to x_1 and T_h (Eq. (5)). Therefore, it is possible to establish a P_t prediction equation similar with Eq. (5). Based on the previously obtained standard fluid database with measured P_h (T_h) we calculated the P_t of HFI using PR-EoS assuming that the HFI was trapped at $T_t = T_h + \Delta T_h$ (ΔT_h is the difference between T_h and T_t). Please note the P_h and fluid compositions are from measured values and the isochore was calculated after volume calibration. Thus, the calculated P_t can be regarded as the true value, which can be used to develop and test the P_t prediction models. Because an isochore can be constrained by any two *P-T* conditions along an isochore pathway, the isochore at homogenization condition (P_h, T_h) of HFI can be obtained if another *P-T* trapping condition is known. Here we firstly calculated P_h at varying T_h ranging from 30 °C to 170 °C based on the previous fluid composition database and then a ΔT_h of 15 °C was artificially selected to calculate the P_{T_h+15} ($T_t = T_h + 15$ °C). Finally, the P_{T_h+15} prediction model fitted by a total of 4444 x_1-T_h-P_{T_h+15} data pairs is shown in the following:

$$P_{T_h+15} = a + bx_1 + cT_h + dx_1^2 + eT_h^2 + fx_1^3 + gT_h^3 + hx_1T_h + ix_1^2T_h + jx_1T_h^2 \quad (9)$$

where the coefficients a, b, c, d, e, f, g, h, i and j are listed in Table 4. Eq. (9) can be used to calculate the P_t of HFI which homogenizes into liquid phase at $T_t = T_h + 15$ °C, with an AAD of ~8.6% for 4444 data (Table 5). Like Eq. (5) Eq. (9) has a better predictive accuracy for hydrocarbon fluid with $x_{7+} > 12.5\%$ and $x_1 < 62\%$ (AAD = 7.1%) and has a relatively low predictive accuracy for gas condensate fluids ($x_{7+} < 12.5\%$) (AAD = 12.6%). Therefore, the isochore slope k at T_h can be calculated by Eq. (10) and any P_t at the isochore can be obtained by Eq. (11),

$$k = \left(P_{T_h+15} - P_{T_h}\right)/15 \quad (10)$$

$$P_t = P_{T_h} + k(T_t - T_h) \quad (11)$$

where the P_{T_h} is the homogenization pressure at T_h which can be calculated through Eq. (5) and T_t is the trapping temperature of the HFI which is usually constrained by the T_h of cogenetic aqueous fluid inclusions with HFI.

The trapping pressure prediction using Eq. (11) only needs the x_1 in HFI, which is superior to the traditional methods (Aplin et al., 2000; Thiéry et al., 2002) because the latter still need other compositions (e.g., C_2–C_{7+} hydrocarbons) to perform *PVT* modeling. Furthermore, the x_1 in HFI can be predicted using Eqs. (1)–(4) which are only related to the F_v and T_h of HFI. This means that once the F_v and T_h of HFI are measured the molar contents of C_{7+} and C_1, P_h ($T = T_h$) and P_t ($T = T_t$) all are available. However, we noticed that the calculated isochore slope k could have a negative value because of relatively low predictive accuracy of Eq. (5) and Eq. (9) for the gas condensate fluids (Table 5), which would result in greater deviation of P_t prediction with increasing of difference between the T_h of HFI and cogenetic aqueous fluid inclusion. After calculating the isochore at bubble point pressure of gas condensate (equivalent to HFI homogenizing into liquid phase) using the PR EoS, we found the isochore k can be well correlated to MW of C_{7+} and the T_h (homogenizing into liquid phase) of gas condensate. The equation for calculating k is shown as following,

$$k = a + bMW_{7+} + cT_h + dMW_{7+}^2 + eT_h^2 + fMW_{7+}^3 + gT_h^3 + hMW_{7+}T_h + iMW_{7+}^2T_h + jMW_{7+}T_h^2 \quad (12)$$

where the coefficients a, b, c, d, e, f, g, h, i and j are listed in Table 4. The AAD of k prediction is ~4.9% (Table 5). Finally, the trapping pressure can be predicted based on Eq. (11).

Following the method of crude oil we calculated the trapping pressure at $T_t = T_h + 15$ °C (T_h = 30–170 °C) for gas condensate fluids after dew point pressure matching and volume calibration. Similar to Eq. (6), a total of 5710 data pairs including molar content of C_1 to C_{7+} and MW and SG of C_{7+} composition are used to extrapolate the trapping pressure prediction equation at $T_t = T_h + 15$ °C (P_{T_h+15}), which is shown in Eq. (13):

$$P_{T_h+15} = ax_1 + bx_2 + cx_3 + dx_4 + ex_1 + fx_2 + gx_3 + hx_4 + i\frac{x_1}{x_{7+}} + jT_h + kx_{7+}MW_{7+} + l(x_{7+}MW_{7+})^2 + m(x_{7+}MW_{7+})^3 + n\frac{MW_{7+}}{SG_{7+}} + o\left(\frac{MW_{7+}}{SG_{7+}}\right)^2 + p\left(\frac{MW_{7+}}{SG_{7+}}\right)^3 + q \quad (13)$$

where the coefficients a, b, c, d, e, f, g, h, i, j, k, l, m, n, o, p and q are listed in Table 4. The SG_{7+} and MW_{7+} are calculated by Eqs. (7) and (8). In contrast with crude oil, Eq. (13) need all the molar composition from C_1 to C_{7+}. The x_{7+} and x_1 content can be predicted based on Eqs. (1)–(4), while other composition (x_2 - x_6) can be obtained using the α-β composition model (Thiéry et al., 2002). The AAD of Eq. (13) is ~19.3% which is slightly higher that P_h prediction from Eq. (6) (AAD = 18.9) (Table 5). Therefore, the trapping pressure of gas condensate inclusions (homogenizing into gas phase) at any trapping temperature can be calculated using Eqs. (10-11). In addition, the isochore slope k for gas condensate inclusions homogenizing into gas phase can also be calculated by the following equation,

$$k = a + bMW_{7+} + cT_h + dMW_{7+}^2 + eT_h^2 + fMW_{7+}^3 + gT_h^3 + hMW_{7+}T_h + iMW_{7+}^2T_h + jMW_{7+}T_h^2 \quad (14)$$

where the coefficients a, b, c, d, e, f, g, h, i and j are listed in Table 4. For HFI which homogenizing into gas phase the isochore k is relatively low with average of ~0.21. The AAD of k prediction using Eq. (14) is ~21.6% (Table 5) for 1547 data. The advantage of k calculation using Eq. (12) and Eq. (14) is that the predictive isochore k is reasonable and avoids negative slopes which is possible to occur using Eq. (10). This is specifically important for P_t prediction if there is a great difference between the T_h and T_t of HFI.

3.4. Strategy and recommendations for P-T reconstructions of HFIs

In the previous sections we have developed several empirical equations to predict hydrocarbon fluid composition including x_1 and x_{7+}, P_h ($T = T_h$), P_t ($T = T_h + 15$ °C), and isochore k for varying HFIs. As the P_h prediction is significantly related to fluid composition (black oil, volatile oil and gas condensate) and phase state (homogenizing into liquid phase or gas phase) when the HFI is trapped, the P_t prediction should consider the types of HFI and phase behavior. Here we divide the HFI into two types based on the phase state after homogenization including oil inclusion (homogenizing into liquid phase, HFI_L) and gas condensate inclusion (homogenizing into gas phase, HFI_G), while the oil inclusions can be further divided into two types based on the composition including normal oil (black oil and volatile oil, $x_{7+} > 12.5\%$), OFI_L and

gas condensate (x_{7+}≤12.5%), $GCFI_L$. Therefore, different HFI should have different strategy for *P-T* conditions reconstruction. Fig. 7 summarizes the procedure for P_t and composition reconstruction with only three measured parameters (F_v, T_h of HFI and coeval aqueous fluid inclusion if the aqueous fluid is saturated with methane). For any HFI of interest, the T_h and F_v at 20 °C should be measured first. If the HFI homogenizes into gas phase then the x_{7+} is directly calculated using Eq. (2). If the HFI homogenizes into liquid phase the T_h vs F_v diagram (Fig. 4) is applied to roughly determine x_{7+}. If the x_{7+} is higher than 20% then Eq. (1) is used to calculate the x_{7+}. If not Eq. (2) is used. The x_1 for any HFI can be predicted by Eq. (3). For HFI_G the whole hydrocarbon composition can be calculated based on the α-β composition model and the MW and SG of C_{7+} composition are calculated using Eqs. (7) and (8). The strategy of P_t prediction for different types HFI is elaborated in the following.

The P_h ($T = T_h$) and P_t at $T = T_h$+15 °C for OFI_L with x_{7+} >12.5% can be predicted with a good accuracy (Table 5), therefore, the best method is to directly calculate the isochore slope *k* using Eq. (10) from Eq. (5) and Eq. (9) and then calculate the P_t using Eq. (11). If the true x_{7+} and x_1 are used the AAD of P_t prediction is ~8.2% based on 1190 standard P_t data, which is better than that from PR-EoS (AAD = 12.1%) (Table 6). In fact, for natural fluid inclusions we do not exactly know the molar content of C_1 and C_{7+} and just estimate them using the empirical equations based on the only measured F_v. To evaluate the predictive accuracy for natural HFI, we assume that the C_{7+} can be determined accurately and then the x_1 is calculated using the empirical equation Eq. (3) and other composition are calculated using the α-β composition model. Finally, an AAD of 12.3% is obtained using the empirical

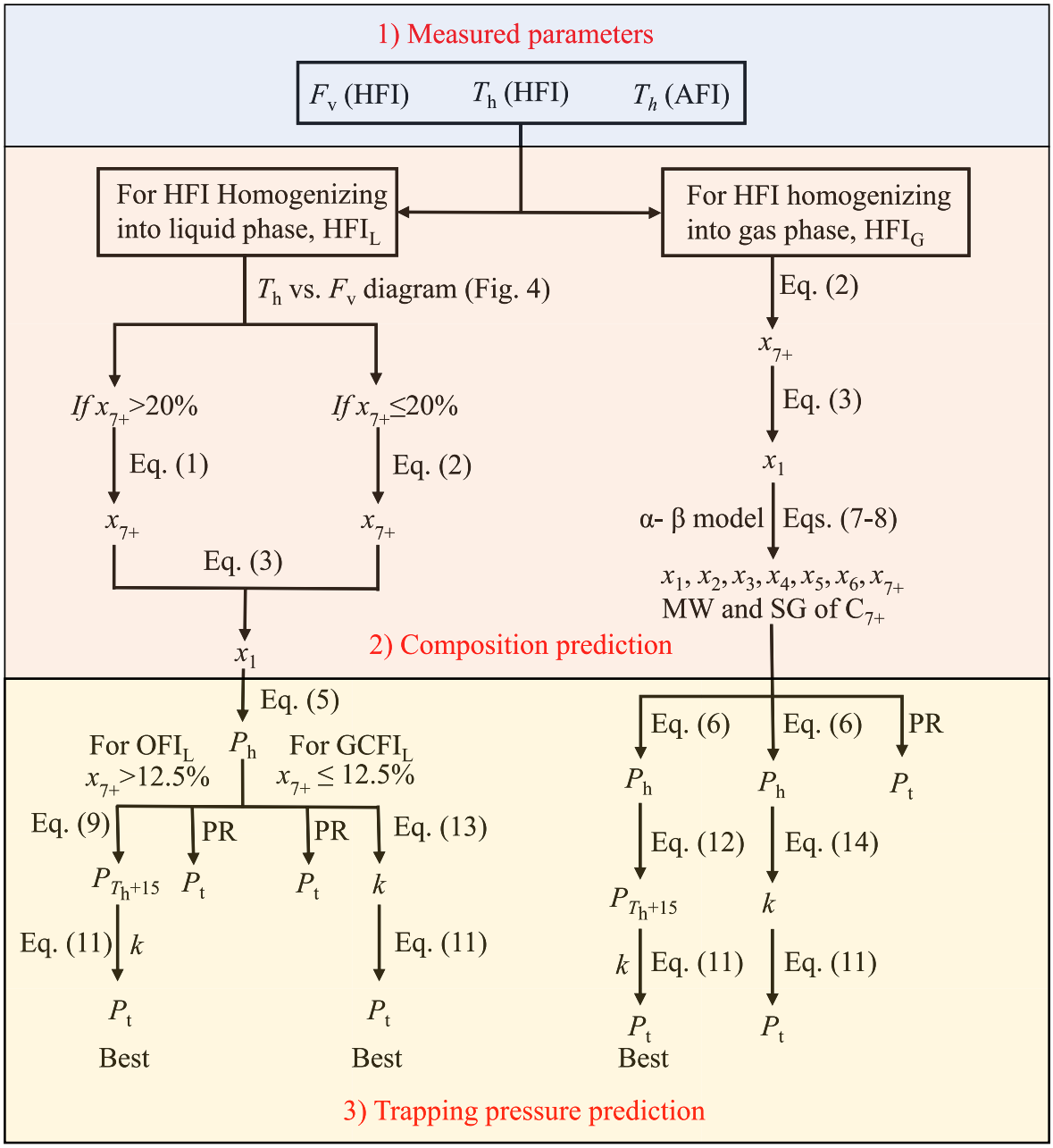

Fig. 7. Procedures for composition prediction and P_t reconstruction of HFI. AFI is the coeval aqueous fluid inclusion with HFI during trapping. OFI_L is oil-bearing fluid inclusion which homogenizes into liquid phase, $GCFI_L$ is gas condensate-bearing fluid inclusion which homogenizes into liquid phase, HFI_G is hydrocarbon fluid inclusion which homogenizes into gas phase. *k* is the isochore slope of HFI. PR is Peng and Robinson (1976) EoS. P_h is homogenization pressure at $T = T_h$, P_{Th+15} is trapping pressure at $T_t = T_h$+15. All the equations and figures shown in Fig. 7 are from this study.

Table 6

P_t prediction accuracy of various strategies for different HFI. OFI_L: oil-bearing fluid inclusion which homogenizes into liquid phase; HFI_G: hydrocarbon fluid inclusions which homogenizes into gas phase; Eq: Equation in this study; MIN: minimum; MAX: maximum; AD: absolute deviation; AAD: average absolute deviation.

$OFI_L$with x_{7+}>12.5%					$GCFI_L$with x_{7+}<12.5%				HFI_G with x_{7+}<12.5%				
	True x_1, Eq	True composition, PR-EoS	True x_{7+}, calculated x_1, Eq	True x_{7+}, calculated other composition, PR-EoS	True composition with calculated MW_{7+} and SG_{7+}, Eq for P_h and k	True x_{7+}, calculated other compositions and MW_{7+} and SG_{7+}, Eq P_h and k	True composition with calculated MW_{7+} and SG_{7+}, PR-EoS	True x_{7+}, calculated other compositions and MW_{7+} and SG_{7+}, PR-EoS	True composition with calculated MW_{7+} and SG_{7+}, Eq for P_h and P_t ($T = T_h$+15)	True composition with calculated MW_{7+} and SG_{7+}, PR-EoS	True x_{7+}, calculated other compositions and MW_{7+} and SG_{7+}, Eq P_h and P_t ($T = T_h$+15)	True x_{7+}, calculated other compositions and MW_{7+} and SG_{7+}, PR-EoS	True x_{7+}, calculated other compositions and MW_{7+} and SG_{7+}, Eq for P_h and k
N	1190	1190	1190	1190	2183	2183	2538	2538	3855	3855	3870	3855	3870
MIN AD	0.01	0.01	0.05	0.01	0	0	0.01	0.015	0	0.02	0.02	0.10	0
MAX AD	88.2	141.1	68.9	52.9	84.2	122.5	99.5	90.2	127.6	103.9	126.0	154.3	104.6	132.8
AAD	8.2	12.1	12.3	14.2	13.2	17.6	11.2	19.0	15.9	25.6	21.2	22.8	30.2	24.6

equations (Eq. (5), Eq. (9) and Eqs. (10-11)) in this study. It is interesting that the PR-EoS has a slightly lower predictive accuracy (AAD = 14.2%) than that from empirical equations (Table 6), which indicates that 1) the *P-T* characteristics are mainly controlled by x_1 for normal crude oil inclusions, 2) our x_1 prediction model is highly effective.

For the $GCFI_L$ with x_{7+} ≤12.5%, the *PVT* phase behaviors are controlled by many other factors and therefore several parameters have been incorporated in the equations, which results in relatively low predictive accuracy (Table 6). As a result, we do not recommend to predict the P_t using Eqs. (9-11), but we suggest obtaining the isochore slope k using Eq. (12) and the calculate the P_t using Eq. (11), or directly calculate the P_t using PR-EoS. The predictive accuracy using empirical equations (AAD = 17.6%) is a little superior to that from EoS (AAD = 19.0%) for predictive fluid compositions (Table 6).

Three methods can be used to calculate the P_t of HFI_G with x_{7+}≤12.5% including P_h-P_t ($T = T_h$+15 °C) empirical equations, P_h-k empirical equations, and pure EoS method. For true fluid composition, P_h-P_t ($T = T_h$+15 °C) method gives a best predictive accuracy with AAD = 15.9% and other two methods have relatively low predictive accuracy with AAD 25.6% and 21.2%, respectively (Table 6). However, for the calculated fluid compositions, the P_h-P_t ($T = T_h$+15 °C) has the best predictive accuracy with AAD of 22.8% which is slightly higher than the P_h-k methods (AAD = 24.6%). The EoS method has the lowest predictive ability (AAD = 30.2%).

Generally, the *P-T* predictive accuracy of HFI have been greatly improved by a large number of measured fluid composition and pressure data. To our knowledge, our models could give the best predictive accuracy for fluid composition and P_t prediction relative to the traditional methods. Furthermore, our models are easy to use. Please note our P_t prediction models are suitable for the HFI which single non-hydrocarbon gas (N_2, CO_2 and H_2S) content is lower than 10 mol%. The presence of water in HFI has been proved by FT-IR measurements (Pironon et al., 2000), however, it seems that the dissolved water in petroleum does not drastically modify *P-T* properties of the HFI in oil window temperature range (typically <150–160 °C) (Pironon et al., 2000; Thiéry et al., 2002). For gas condensate, the presence of brine could slightly increase the dew point pressure by around 2% or has no impact on it relative to the system without brine (Yushchenko and Brusilovsky, 2016). If the gas condensate contains a large amounts of high water-soluble hydrogen sulfide or carbon dioxide, the effect of brine on the *PVT* phase behaviors could not be neglected (Yushchenko and Brusilovsky, 2016). Moreover, the dissolved water in petroleum is too low to be observed microscopically. Therefore, for ordinary petroleum coexisting with aqueous fluid, trapping pressure and temperature are generally obtained by intersection between petroleum and aqueous inclusions isochores without considering the effect of water (Bourdet et al., 2012; Bourdet et al., 2010; Guillaume et al., 2003; Narr and Burruss, 1984).

Our models can also be used to calculate the *P-T* trapping condition of HFIs if the coeval aqueous fluid inclusions are not saturated with methane. Under this situation the isochore of aqueous fluid inclusion must be determined and then the trapping conditions can be determined by the intersection of isochores of HFI and coeval aqueous fluid inclusion (Bourdet et al., 2014; Pironon, 2020), where the isochore of HFI can be calculated based on our new methods following the recommendations in Fig. 7. For the methane saturated HFI, the trapping condition of HFI is equivalent to its homogenization condition ($T_t = T_h$ and P_t=P_h), thus the best prediction accuracy of P_t can be obtained for oil inclusions and gas condensate inclusions with AAD 7.3% and 12.7%, respectively (Table 5). An Excel program attached in the supplementary data which has been developed to allow calculating the fluid compositions (C_1, C_2, C_3, C_4, C_5, C_6, C_{7+}), homogenization pressure (P_h), single-phase isochore slope k and trapping condition (P_t) of HFI based on the procedures in Fig. 7, and it can be applied routinely on different case studies.

4. Conclusions

Based on a large number of measured composition, pressure and volume data of crude oil and gas condensate, new fluid composition (x_1 and x_{7+}) prediction models have been developed. The new composition prediction models only need the F_v and T_h of HFI, which makes quantitative comparation of different generations of HFI composition possible in a F_v vs. T_h diagram. Through matching measured saturation pressure and volume calibration standard database are established including fluid composition, homogenization pressure, trapping pressure. The database covers a wide range of composition and pressure and therefore can represent HIFs in varying origin and source. For HFIs homogenizing into liquid phase with x_{7+} >12.5% only x_1 is enough to obtain a good prediction accuracy of P_t reconstruction (AAD = 8.2–12.3%). For the gas condensate fluid inclusions, more compositional detail (x_1-x_{7+}) together with the physical property (MW and SG) of C_{7+} composition must be incorporated into the prediction model to obtain a better prediction accuracy of P_t. This is the case regardless of whether the gas condensate inclusions homogenize into the liquid or the vapor phase. Although many parameters are used to developed the new P_t prediction model, only the F_v of HFI is a measured value and others are derived from empirical equations, an advantage to previous methods. The new models give prediction accuracy of 11.2–17.6% (AAD) for gas condensate fluid inclusions which homogenize into liquid phase, and 15.9–22.8% (AAD) for gas condensate fluid inclusions which homogenize into gas phase. Our new composition and P_t prediction models can give the best and fastest prediction of hydrocarbon fluid composition and trapping conditions and are of great significance for petroleum charging history reconstruction in sedimentary basins.

Declaration of competing interest

The authors declare that they have no known competing financial interests or personal relationships that could have appeared to influence the work reported in this paper.

Data availability

Data will be made available on request.

Acknowledgments

This work was supported by the National Natural Science Foundation of China (NSFC; grant numbers 42072176 and 42272169) and PetroChina Innovation Foundation (grant number 2019D-5007-0105). We thank Zhi Zhong and Afshin Tatar for providing composition and saturation pressure data. We thank Xin Yang, Bo Xiang, Xiaoting Xu and Shaoqin Li for assistance with data collection. Herbert Volk, and two anonymous reviewers are gratefully acknowledged for their constructive reviews and comments on the paper.

Nomenclature

T	Temperature (°C)
P	Pressure (MPa)
T_h	Homogenization temperature (°C)
P_h	Homogenization pressure (MPa)
F_v	Degree of bubble filling (%)
P_t	Trapping pressure (MPa)
P_{T_h+15}	Trapping pressure at T_h +15 °C (MPa)
P_s	Saturation pressure (MPa)
P_b	Bubble point pressure (MPa)
P_d	Dew point pressure (MPa)
T_t	Trapping temperature (°C)
k	Isochore slope
x_i	Mole percentage of single component (or pseudo-component) i (%)
MW	Molar weight (g/mol)
SG	Specific gravity
AD	Absolute deviation (%) defined by AD $= \left\|\frac{X^{cal}-X^{exp}}{X^{exp}}\right\| \times 100\%$, where X^{cal} represents calculated molar content or pressure and the X^{exp} is the experimentally measured molar content or pressure
AAD	Average absolute deviation (%) defined by AAD $= \frac{\sum_1^N AD}{N}$, where, N is samples number

Appendix A. Supplementary data

Supplementary data to this article can be found online at https://doi.org/10.1016/j.marpetgeo.2023.106403.

References

Agarwal, R., Li, Y., Nghiem, L., 1990. A regression technique with dynamic parameter selection for phase-behavior matching. SPE Reservoir Eng. 5 (1), 115–120.
Aghamiri, S., Tamtaji, M., Ghafoori, M.J., 2018. Developing a K-value equation for predict dew point pressure of gas condensate reservoirs at high pressure. Petroleum 4 (4), 437–443.
Ahmadi, M.A., Ebadi, M., Yazdanpanah, A., 2014. Robust intelligent tool for estimating dew point pressure in retrograded condensate gas reservoirs: application of particle swarm optimization. J. Petrol. Sci. Eng. 123, 7–19.
Ahmed, T., 1989. Hydrocarbon Phase Behavior. Gulf Pub. Co., Houston.
Ahmed, T., Cady, G., Story, A., 1985. A generalized correlation for characterizing the hydrocarbon heavy fraction. In: SPE Annual Technical Conference and Exhibition. SPE, Las Vegas, Nevada, 14266. MS.
Akpabio, J.U., Udofia, E.E., Ogbu, M., 2014. PVT fluid characterization and consistency check for retrograde condensate reservoir modeling. SPE Nigeria Annual International Conference and Exhibition.
Al-Dhamen, M., Al-Marhoun, M., 2011. New Correlations for Dew-point Pressure for Gas Condensate, SPE Saudi Arabia Section Young Professionals Technical Symposium.
Al-Mahroos, F.M., Tjoa, G.H., 1985. Analysis and Phase Behavior of Khuff Gas System. SPE, 15766.
Al-Meshari, A., 2004. New Strategic Method to Tune Equation-Of-State to Match Experimental Data for Compositional Simulation. Texas A&M University, p. 248.

Al-Meshari, A.A., Armco, S., MaCain, W.D., 2007a. Validation of splitting the hydrocarbon plus fraction: first step in tuning equation-of-state. In: SPE Middle East Oil and Gas Show and Conference. SPE, Kingdom of Bahrain, 104631.
Al-Meshari, A.A., Kokal, S.L., Al-Muhainy, A.M., Ali, M.S., 2007b. Measurement of Gas Condensate, Near-Critical and Volatile Oil Densities and Viscosities at Reservoir Conditions. SPE Annual Technical Conference and Exhibition.
Alarouj, M., Alomair, O., Elsharkawy, A., 2020. Gas condensate reservoirs: characterization and calculation of dew-point pressure. Petrol. Explor. Dev. 47 (5), 1091–1102.
Alderton, D.H.M., Bevins, R.E., 1996. P-T conditions in the South Wales Coalfield: evidence from coexisting hydrocarbon and aqueous fluid inclusions. J. Geol. Soc. 153 (2), 265–275.
Ali, M.T., El-Banbi, A.H., 2015. EOS Tuning – Comparison between Several Valid Approaches and New Recommendations. SPE North Africa Technical Conference and Exhibition.
Almehaideb, R., Al-Khanbashi, A., Abdulkarim, M., Ali, M., 2000. EOS tuning to model full field crude oil properties using multiple well fluid PVT analysis. J. Petrol. Sci. Eng. 26 (1–4), 291–300.
Almehaideb, R.A., Abdulkarim, M.A., Al-Khanbashi, A.S., 2001. Improved K-values correlation for UAE crude oil components at low pressures using PVT laboratory data. Fuel 80 (1), 117–124.
Almehaideb, R.A., Abdulkarim, M.A., Ashour, I., Abdullatif, M.A., 2004. Application of the PR-EoS with C_{7+} splitting to model fluid properties in a large two-phase petroleum reservoir. Petrol. Sci. Technol. 22 (11), 1465–1489.
Aplin, A.C., Larter, S.R., Bigge, M.A., Macleod, G., Swarbrick, R.E., Grunberger, D., 2000. Confocal microscopy of fluid inclusions reveals fluid-pressure histories of sediments and an unexpected origin of gas condensate. Geology 28 (11), 1047–1050.
Aplin, A.C., Macleod, G., Larter, S.R., Pedersen, K.S., Sorensen, H., Booth, T., 1999. Combined use of Confocal Laser Scanning Microscopy and PVT simulation for estimating the composition and physical properties of petroleum in fluid inclusions. Mar. Petrol. Geol. 16 (2), 97–110.
Arabloo, M., Rafiee-Taghanaki, S., 2014. SVM modeling of the constant volume depletion (CVD) behavior of gas condensate reservoirs. J. Nat. Gas Sci. Eng. 21, 1148–1155.
Assareh, M., Pishvaei, M., Ghotbi, S., 2011. Application of simulated annealing technique to non-linear optimization of PC-SAFT for petroleum reservoir fluids. Journal of Petroleum Science and Technology 1 (1), 3–14.
Avaullée, L., Duchet-Suchaux, P., Durandeau, M., Jaubert, J.N., 2001. A new approach in correlating the oil thermodynamic properties. J. Petrol. Sci. Eng. 30 (1), 43–65.
Avaullee, L., Neau, E., Jaubert, J.-N., 1997. Thermodynamic modeling for petroleum fluids II. Prediction of PVT properties of oils and gases by fitting one or two parameters to the saturation pressures of reservoir fluids. Fluid Phase Equil. 139 (1–2), 171–203.
Bakker, R.J., Diamond, L.W., 2006. Estimation of volume fractions of liquid and vapor phases in fluid inclusions, and definition of inclusion shapes. Am. Mineral. 91, 635–657.
Behar, F., Lorant, F., Mazeas, L., 2008. Elaboration of a new compositional kinetic schema for oil cracking. Org. Geochem. 39 (6), 764–782.
Bonyadi, A., Esmaeilzadeh, F., 2007. Prediction of gas condensate properties by Esmaeilzadeh-Roshanfekr equation of state. Fluid Phase Equil. 260 (2), 326–334.
Boreham, C.J., Edwards, D.S., Hope, J.M., Chen, J., Hong, Z., 2008. Carbon and hydrogen isotopes of neo-pentane for biodegraded natural gas correlation. Org. Geochem. 39 (10), 1483–1486.
Bourdet, J., Burruss, R.C., Chou, I.M., Kempton, R., Liu, K.Y., Hung, N.V., 2014. Evidence for a palaeo-oil column and alteration of residual oil in a gas-condensate field: integrated oil inclusion and experimental results. Geochem. Cosmochim. Acta 142, 362–385.
Bourdet, J., Eadington, P., Volk, H., George, S.C., Pironon, J., Kempton, R., 2012. Chemical changes of fluid inclusion oil trapped during the evolution of an oil reservoir: jabiru-1A case study (Timor Sea, Australia). Mar. Petrol. Geol. 36 (1), 118–139.
Bourdet, J., Pironon, J., Levresse, G., Tritlla, J., 2008. Petroleum type determination through homogenization temperature and vapour volume fraction measurements in fluid inclusions. Geofluids 8 (1), 46–59.
Bourdet, J., Pironon, J., Levresse, G., Tritlla, J., 2010. Petroleum accumulation and leakage in a deeply buried carbonate reservoir, Níspero field (Mexico). Mar. Petrol. Geol. 27 (1), 126–142.
Burruss, R.C., 2003. Raman microspectrometry of fluid inclusion. In: Samson, I., Anderson, A., Marshall, D. (Eds.), Fluid Inclusions: Analysis and Interpretation. Mineralogical Association of Canada Short Course Series. Mineralogical Association of Canada Short Course Series, pp. 279–290.
Burruss, R.C., Slepkov, A.D., Pegoraro, A.F., Stolow, A., 2012. Unraveling the complexity of deep gas accumulations with three-dimensional multimodal CARS microscopy. Geology 40 (12), 1063–1066.
Caumon, M.-C., Robert, P., Laverret, E., Tarantola, A., Randi, A., Pironon, J., Dubessy, J., Girard, J.-P., 2014. Determination of methane content in NaCl–H_2O fluid inclusions by Raman spectroscopy. Calibration and application to the external part of the Central Alps (Switzerland). Chem. Geol. 378–379, 52–61.
Cavett, R., 1962. Physical data for distillation calculations–vapor-liquid equilibria. In: Proc. 27th Annual Meeting. American Petroleum Institute, Dallas, pp. 351–366.
Coats, K.H., 1985. Simulation of gas condensate reservoir performance. J. Petrol. Technol. 37 (10), 1870–1886.
Coats, K.H., Smart, G.T., 1986. Application of a regression-based EoS PVT program to laboratory data. SPE Reservoir Eng. 1 (3), 277–299.
Danesh, A., 1998. In: PVT and Phase Behaviour of Petroleum Reservoir Fluids. Developments in Petroleum Science, vol. 47. Elsevier, Amsterdam, the Netherlands.
Danesh, A., Xu, D., Todd, A., 1992. A grouping method to optimize oil description for compositional simulation of gas-injection processes. SPE Reservoir Eng. 7 (3), 343–348.
Donohoe, C.W., Buchanan Jr., R.D., 1981. Economic evaluation of cycling gas-condensate reservoirs with nitrogen. J. Petrol. Technol. 33 (2), 263–270.
Drohm, J.K., Goldthorpe, W.H., Trengove, R., 1988. Enhancing the Evaluation of PVT Data. Offshore South East Asia Show, Singapore, 17685. MS.
Duan, Z., Møller, N., Greenberg, J., Weare, J.H., 1992. The prediction of methane solubility in natural waters to high ionic strength from 0 to 250°C and from 0 to 1600 bar. Geochem. Cosmochim. Acta 56 (4), 1451–1460.
Dubessy, J., Buschaert, S., Lamb, W., Pironon, J., Thiéry, R., 2001. Methane-bearing aqueous fluid inclusions: Raman analysis, thermodynamic modelling and application to petroleum basins. Chem. Geol. 173 (1–3), 193–205.
El-Banbi, A.H., Fattah, K.A., Sayyouh, H., 2006. New Modified Black-Oil PVT Correlations for Gas Condensate and Volatile Oil Fluids. SPE Annual Technical Conference and Exhibition.
Elsharkawy, A.M., 2002a. Eos's calculations of volumetric and transport properties of sour gases and gas condensates. The 6th Saudi Engineering Conference, KFUPM, Dhahran 2, 509–536.
Elsharkawy, A.M., 2002b. Predicting the dew point pressure for gas condensate reservoirs: empirical models and equations of state. Fluid Phase Equil. 193 (1–2), 147–165.
Elsharkawy, A.M., 2002c. Predicting the properties of sour gases and condensates: equations of state and empirical correlations. SPE International Petroleum Conference and Exhibition in Mexico.
Elsharkawy, A.M., 2003. An empirical model for estimating the saturation pressures of crude oils. J. Petrol. Sci. Eng. 38 (1–2), 57–77.
England, W., Mackenzie, A., Mann, D., Quigley, T., 1987. The movement and entrapment of petroleum fluids in the subsurface. J. Geol. Soc. 144 (2), 327–347.
Ferket, H., Guilhaumou, N., Roure, F., Swennen, R., 2011. Insights from fluid inclusions, thermal and PVT modeling for paleo-burial and thermal reconstruction of the cordoba petroleum system (Ne Mexico). Mar. Petrol. Geol. 28 (4), 936–958.
Firoozabadi, A., Hekim, Y., Katz, D.L., 1978. Reservoir depletion calculations for gas condensates using extended analyses in the peng-robinson equation of state. Can. J. Chem. Eng. 56 (5), 610–615.
Firoozabadi, A., Katz, D.L., 1988. Surface tension of reservoir crudeoil/gas systems recognizing the asphalt in the heavy fraction. SPE Reservoir Eng. 3 (1), 265–272.
Folsta, K.C.B.M., Camargo, G.M., Espósito, R.O., 2010. Gas condensate characterization from chromatogram areas and retention times. Fluid Phase Equil. 292 (1), 87–95.
George, S.C., Krieger, F.W., Eadington, P.J., Quezada, R.A., Greenwood, P.F., Eisenberg, L.I., Hamilton, P.J., Wilson, M.A., 1997. Geochemical comparison of oil-bearing fluid inclusions and produced oil from the Toro Sandstone, Papua New Guinea. Org. Geochem. 26 (3–4), 155–173.
George, S.C., Lisk, M., Summons, R.E., Quezada, R.A., 1998. Constraining the oil charge history of the South Pepper oilfield from the analysis of oil-bearing fluid inclusions. Org. Geochem. 29 (1–3), 631–648.
George, S.C., Ruble, T.E., Dutkiewicz, A., Eadington, P.J., 2001. Assessing the maturity of oil trapped in fluid inclusions using molecular geochemistry data and visually-determined fluorescence colours. Appl. Geochem. 16 (4), 451–473.
George, S.C., Volk, H., Ahmed, M., 2007. Geochemical analysis techniques and geological applications of oil-bearing fluid inclusions, with some Australian case studies. J. Petrol. Sci. Eng. 57 (1–2), 119–138.
George, S.C., Volk, H., Dutkiewicz, A., Ridley, J., Buick, R., 2008. Preservation of hydrocarbons and biomarkers in oil trapped inside fluid inclusions for >2 billion years. Geochem. Cosmochim. Acta 72 (3), 844–870.
Godwin, O.N., 2012. A New analytical method for predicting dew point pressures for gas condensate reservoirs. Nigeria Annual International Conference and Exhibition.
Guillaume, D., Teinturier, S., Dubessy, J., Pironon, J., 2003. Calibration of methane analysis by Raman spectroscopy in H_2O-NaCl-CH_4 fluid inclusions. Chem. Geol. 194 (1–3), 41–49.
Guo, P., Liu, H., Wang, C., Du, J., Fan, B., Jing, M., Wang, Z., Deng, Z., Zhan, S., 2020. The determination of phase behavior properties of high-temperature high-pressure and rich condensate gases. Fuel 280, 118568.
Haghtalab, A., Mahmoodi, P., Mazloumi, S.H., 2011. A modified Peng-Robinson equation of state for phase equilibrium calculation of liquefied, synthetic natural gas, and gas condensate mixtures. Can. J. Chem. Eng. 89 (6), 1376–1387.
Haji-Savameri, M., Menad, N.A., Norouzi-Apourvari, S., Hemmati-Sarapardeh, A., 2020. Modeling dew point pressure of gas condensate reservoirs: comparison of hybrid soft computing approaches, correlations, and thermodynamic models. J. Petrol. Sci. Eng. 184, 106558.
Hanor, J.S., 1980. Dissolved methane in sedimentary brines; potential effect on the PVT properties of fluid inclusions. Econ. Geol. 75 (4), 603–609.
Hassan, A.M., Mahmoud, M.A., Al-Majed, A.E., Elkatatny, S.M., Al-Nakhli, A.R., Bataweel, M.A., 2018. Effect of In-Situ Generation of Heat and Pressure on Phase Behavior of Gas Condensate, SPE Kingdom of Saudi Arabia Annual Technical Symposium and Exhibition.
Haszeldine, R., Samson, I., Cornford, C., 1984. Dating diagenesis in a petroleum basin, a new fluid inclusion method. Nature 307, 354–357.
Hode, T., Zebühr, Y., Broman, C., 2006. Towards biomarker analysis of hydrocarbons trapped in individual fluid inclusions: first extraction by ErYAG laser. Planet. Space Sci. 54 (15), 1575–1583.
Hoffman, A., Crump, J., Hocott, C., 1953. Equilibrium Constants for a Gas-Condensate System, vol. 198. Transaction of American Institute of Mining, Metallurgical, and Petroleum Engineers, pp. 1–10.

Hong, K., 1982. Lumped-component Characterization of Crude Oils for Compositional Simulation, SPE Enhanced Oil Recovery Symposium. SPE, Tulsa, Oklahoma, 10691. MS.
Hou, D., Jia, Y., Shi, Y., Zhao, R., Tang, H., Sun, L., 2020. Experimental study on the effect of CO_2 on phase behavior characteristics of condensate gas reservoir. J. Chem. 2020, 6041081.
Hou, D.L., Xiao, Y., Pan, Y., Sun, L., Li, K., 2016. Experiment and simulation study on the special phase behavior of huachang near-critical condensate gas reservoir fluid. J. Chem.
Huang, S.S.S., Leu, A.D., Ng, H.J., Robinson, D.B., 1985. The phase behavior of two mixtures of methane, carbon dioxide, hydrogen sulfide, and water. Fluid Phase Equil. 19 (1), 21–32.
Hubbert, M.K., 1953. Entrapment of petroleum under hydrodynamic conditions. AAPG (Am. Assoc. Pet. Geol.) Bull. 37 (8), 1954–2026.
Ibeh, S.U., Chubueze, S.E., 2016. PVT analysis: validity checks and EoS tuning techniques for retrograde gas condensate reservoirs. SPE Nigeria Annual International Conference and Exhibition.
Imo-Jack, O., 2010. PVT Characterization of a gas condensate reservoir and investigation of factors affecting deliverability. Nigeria Annual International Conference and Exhibition.
Jacopy, R.H., Berry, V.J., 1958. A method for predicting pressure maintenance for reservoirs producing volatile oil. Petroleum Transactions, Transaction of American Institute of Mining, Metallurgical, and Petroleum Engineers 213, 59–65.
Jamaluddin, A.K.M., Creek, J., Kabir, C.S., McFadden, J.D., D'Cruz, D., Joseph, M.T., Joshi, N., Ross, B., 2001. A comparison of various laboratory techniques to measure thermodynamic asphaltene instability. SPE Asia Pacific Improved Oil Recovery Conference.
Jarrahian, A., Moghadasi, J., Heidaryan, E., 2015. Empirical estimating of black oils bubblepoint (saturation) pressure. J. Petrol. Sci. Eng. 126, 69–77.
Jaubert, J.-N., Avaullee, L., Souvay, J.-F., 2002a. A crude oil data bank containing more than 5000 PVT and gas injection data. J. Petrol. Sci. Eng. 34 (1–4), 65–107.
Jaubert, J.-N., Neau, E., 2002. Characterization of heavy oils. 2. Definition of a significant characterizing parameter to ensure the reliability of predictive methods for PVT calculations. Ind. Eng. Chem. Res. 34 (5), 1873–1881.
Jaubert, J.-N., Neau, E., Avaullee, L., Zaborowski, G., 1995. Characterization of heavy oils. 3. Prediction of gas injection behavior: swelling test, multicontact test, multiple-contact minimum miscibility pressure, and multiple-contact minimum miscibility enrichment. Ind. Eng. Chem. Res. 34 (11), 4016–4032.
Jaubert, J.-N., Neau, E., Peneloux, A., Fressigne, C., Fuchs, A., 2002b. Phase equilibrium calculations on an Indonesian crude oil using detailed NMR analysis or a predictive method to assess the properties of the heavy fractions. Ind. Eng. Chem. Res. 34 (2), 640–655.
Jaubert, J.-N., Solimando, R., Paricaud, P., Barreau, A., 2000. Use of distribution functions: a useful tool to calculate the properties of condensate gases. Ind. Eng. Chem. Res. 39 (12), 5029–5036.
Jhaveri, B., Youngren, G., 1988. Three-parameter modification of the Peng-Robinson equation of state to improve volumetric predictions. SPE Reservoir Eng. 3 (3), 1033–1040.
Jia, H., Wu, X., 2017. Killing fluid loss mechanism and productivity recovery in a gas condensate reservoir considering the phase behavior change. Petrol. Explor. Dev. 44 (4), 659–666.
Joiner, D.S., Long, G.B., 1978. Retrograde GOR Behavior of Condensate Reservoirs from Well Test Data. SPE Annual Fall Technical Conference and Exhibition.
Kamari, A., Sattari, M., Mohammadi, A.H., Ramjugernath, D., 2016. Rapid method for the estimation of dew point pressures in gas condensate reservoirs. J. Taiwan Inst. Chem. Eng. 60, 258–266.
Karlsen, D.A., Nedkvitne, T., Larter, S.R., Bjørlykke, K., 1993. Hydrocarbon composition of authigenic inclusions: application to elucidation of petroleum reservoir filling history. Geochem. Cosmochim. Acta 57 (15), 3641–3659.
Kaydani, H., Mohebbi, A., Hajizadeh, A., 2016. Dew point pressure model for gas condensate reservoirs based on multi-gene genetic programming approach. Appl. Soft Comput. 47, 168–178.
Khodapanah, E., Tabatabaei-Nejad, S.A., 2014. A consistent method for simultaneous calculation of upper and lower dew point pressures of gas condensate fluids. J. Nat. Gas Sci. Eng. 21, 556–567.
Khoshnamvand, Y., Assareh, M., Davoudi, B.M., 2017. Phase behavior modeling for gas condensate fluids with PC-SAFT and an improved binary interaction coefficient model. Fluid Phase Equil. 444, 37–46.
Kilgren, K.H., 1966. Phase behavior of a high-pressure condensate reservoir fluid. J. Petrol. Technol. 18 (8), 1001–1005.
Kokal, S., Al-Dokhi, M., Sayegh, S., 2003. Phase behavior of a gas-condensate/water system. SPE Reservoir Eval. Eng. 6 (6), 412–420.
Krejbjerg, K., Pedersen, K.S., 2006. Controlling VLLE Equilibrium with a Cubic EoS in Heavy Oil Modeling. Canadian International Petroleum Conference.
Lagache, M.H., Ungerer, P., Boutin, A., 2004. Prediction of thermodynamic derivative properties of natural condensate gases at high pressure by Monte Carlo simulation. Fluid Phase Equil. 220 (2), 211–223.
Le, V.-H., Caumon, M.-C., Tarantola, A., Randi, A., Robert, P., Mullis, J., 2020. Calibration data for simultaneous determination of P-V-X properties of binary and ternary CO_2 - CH_4 - N_2 gas mixtures by Raman spectroscopy over 5–600 bar: application to natural fluid inclusions. Chem. Geol. 552, 119783.
Leibovici, C.F., Govel, P.L., Piacentino, T., 1993. A Consistent Procedure for the Estimation of Pseudo-component Properties, SPE Annual Technical Conference and Exhibition.
Li, Y., Nghiem, L., Siu, A., 1985. Phase behavior computations for reservoir fluids: effect of pseudo-components on phase diagrams and simulation results. J. Can. Petrol. Technol. 24 (6), 29–36.
Liu, D.H., Xiao, X.M., Mi, J.K., Li, X.Q., Shen, J.K., Song, Z.G., Peng, P.A., 2003. Determination of trapping pressure and temperature of petroleum inclusions using PVT simulation software–a case study of Lower Ordovician carbonates from the Lunnan Low Uplift, Tarim Basin. Mar. Petrol. Geol. 20 (1), 29–43.
Liu, H., Sun, C.Y., Yan, K.L., Ma, Q.L., Wang, J., Chen, G.J., Xiao, X.J., Wang, H.Y., Zheng, X.T., Li, S., 2013. Phase behavior and compressibility factor of two China gas condensate samples at pressures up to 95 MPa. Fluid Phase Equil. 337, 363–369.
Louli, V., Pappa, G., Boukouvalas, C., Skouras, S., Solbraa, E., Christensen, K.O., Voutsas, E., 2012. Measurement and prediction of dew point curves of natural gas mixtures. Fluid Phase Equil. 334, 1–9.
Majidi, S.M.J., Shokrollahi, A., Arabloo, M., Mahdikhani-Soleymanloo, R., Masihi, M., 2014. Evolving an accurate model based on machine learning approach for prediction of dew-point pressure in gas condensate reservoirs. Chem. Eng. Res. Des. 92 (5), 891–902.
Maleki, M.R., Rashidi, F., Mahani, H., Khamehchi, E., 2012. A simulation study of the enhancement of condensate recovery from one of the Iranian naturally fractured condensate reservoirs. J. Petrol. Sci. Eng. 92–93, 158–166.
Mao, S., Hu, J., Zhang, D., Li, Y., 2013. Thermodynamic modeling of ternary CH_4-H_2O-NaCl fluid inclusions. Chem. Geol. 335, 128–135.
Marruffo, I., Maita, J., Him, J., Gonzalo, R., 2002. Correlations to Determine Retrograde Dew Pressure and C_{7+} Percentage of Gas Condensate Reservoirs on Basis of Production Test Data of Eastern Venezuelan Fields. SPE Gas Technology Symposium.
Mazloom, J., Rashidi, F., Kelly, R., 2004. A novel approach to the calculation of the distance of a sealing fault from a well in a gas condensate reservoir. J. Petrol. Sci. Eng. 45 (3), 149–158.
McCain, W.D.,1990. The properties of petroleum fluids. Pennwell Publishing Company, Tulsa.
McLimans, R.K., 1987. The application of fluid inclusions to migration of oil and diagenesis in petroleum reservoirs. Appl. Geochem. 2 (5–6), 585–603.
Mehrabian, A., Crespo, F., 2011. A new multi-sample EoS model for the gas condensate phase behavior analysis. Oil & Gas Science and Technology-Revue D Ifp Energies Nouvelles 66 (6), 1025–1033.
Moharam, H.M., Fahim, M.A., 1995. Prediction of viscosity of heavy petroleum fractions and crude oils using a corresponding states method. Ind. Eng. Chem. Res. 34 (11), 4140–4144.
Munz, I.A., 2001. Petroleum inclusions in sedimentary basins: systematics, analytical methods and applications. Lithos 55 (1–4), 195–212.
Munz, I.A., Johansen, H., Holm, K., Lacharpagne, J.C., 1999a. The petroleum characteristics and filling history of the Frøy field and the Rind discovery, Norwegian North Sea. Mar. Petrol. Geol. 16 (7), 633–651.
Munz, I.A., Johansen, H., Johanse, I., 1999b. Characterisation of Composition and PVT Properties of Petroleum Inclusions: Implications of Reservoir Filling and Compartmentalisation, SPE Annual Technical Conference and Exhibition. SPE, Houston, Texas, 56519. MS.
Munz, I.A., Wangen, M., Girard, J.-P., Lacharpagne, J.-C., Johansen, H., 2004. Pressure-temperature-time-composition (P-T-t-X) constraints of multiple petroleum charges in the Hild field, Norwegian North Sea. Mar. Petrol. Geol. 21 (8), 1043–1060.
Munz, I.A., Yardley, B.W.D., Banks, D.A., Wayne, D., 1995. Deep penetration of sedimentary fluids in basement rocks from southern Norway: evidence from hydrocarbon and brine inclusions in quartz veins. Geochem. Cosmochim. Acta 59 (2), 239–254.
Najafi-Marghmaleki, A., Tatar, A., Barati-Harooni, A., Choobineh, M.-J., Mohammadi, A. H., 2016. GA-RBF model for prediction of dew point pressure in gas condensate reservoirs. J. Mol. Liq. 223, 979–986.
Narr, W., Burruss, R.C., 1984. Origin of reservoir fractures in little knife field, north Dakota. AAPG (Am. Assoc. Pet. Geol.) Bull. 68 (9), 1087–1100.
Nasrifar, K., Bolland, O., Moshfeghian, M., 2005. Predicting natural gas dew points from 15 equations of state. Energy Fuel. 19 (2), 561–572.
Neau, E., Jaubert, J.N., Rogalski, M., 1993. Characterization of heavy oils. Ind. Eng. Chem. Res. 32 (6), 1196–1203.
Nedkvitne, T., Karlsen, D.A., Bjørlykke, K., Larter, S.R., 1993. Relationship between reservoir diagenetic evolution and petroleum emplacement in the Ula Field, North Sea. Mar. Petrol. Geol. 10 (3), 255–270.
Nemeth, L.K., Kennedy, H.T., 1967. A correlation of dewpoint pressure with fluid composition and temperature. Soc. Petrol. Eng. J. 7 (2), 99–104.
Ng, H.-J., Robinson, D.B., 1986. The Influence of Water and Carbon Dioxide on the Phase Behavior and Properties of a Condensate Fluid. SPE Annual Technical Conference and Exhibition.
Novak, N., Louli, V., Skouras, S., Voutsas, E., 2018. Prediction of dew points and liquid dropouts of gas condensate mixtures. Fluid Phase Equil. 457, 62–73.
Nowroozi, S., Ranjbar, M., Hashemipour, H., Schaffie, M., 2009. Development of a neural fuzzy system for advanced prediction of dew point pressure in gas condensate reservoirs. Fuel Process. Technol. 90 (3), 452–457.
Pedersen, K., Thomassen, P., Fredenslund, A., 1988. On the danger of "tuning" equation of sate parameters. Chem. Eng. Sci. 43 (2), 269–278.
Pedersen, K.S., 2007. PC-SAFT Equation of State Applied to Petroleum Reservoir Fluids. SPE Annual Technical Conference and Exhibition.
Pedersen, K.S., Blilie, A.L., Meisingset, K.K., 1992. PVT calculations on petroleum reservoir fluids using measured and estimated compositional data for the plus fraction. Ind. Eng. Chem. Res. 31 (5), 1378–1384.
Pedersen, K.S., Rasmussen, P., Fredenslund, A., 1985. Thermodynamics of petroleum mixtures containing heavy hydrocarbons. 3. Efficient flash calculation procedures using the SRK equation of state. Ind. Eng. Chem. Process Des. Dev. 24 (4), 948–954.

Pedersen, K.S., Thomassen, P., Fredenslund, A., 1989. Charization of gas condensate mixtures. Advances in Thermodynamics 1, 137–152.
Peng, D., Robinson, D., 1976. A new two-constant equation of state. Industrial & Engineering Chemistry Research Fundamentals 15 (1), 59–64.
Ping, H., Chen, H., George, S.C., 2020a. Quantitatively predicting the thermal maturity of oil trapped in fluid inclusions based on fluorescence and molecular geochemical data of oil inclusions in the Dongying depression, Bohai Bay Basin, China. AAPG (Am. Assoc. Pet. Geol.) Bull. 104 (8), 1751–1791.
Ping, H., Chen, H., Jia, G., 2017a. Petroleum accumulation in the deeply buried reservoirs in the northern Dongying Depression, Bohai Bay Basin, China: new insights from fluid inclusions, natural gas geochemistry, and 1-D basin modeling. Mar. Petrol. Geol. 80, 70–93.
Ping, H., Chen, H., Song, G., Thiéry, R., 2012. Individual oil inclusion composition prediction and its application in oil and gas accumulation studies. Earth Sci. J. China Univ. Geosci. 37 (4), 815, 524 (in Chinese with English abstract).
Ping, H., Chen, H., Thiéry, R., 2013a. Improvement on paleopressure prediction using petroleum inclusions thermodynamic modeling: saturation pressure prediction and volume calibration. Earth Sci. J. China Univ. Geosci. 38 (1), 143–155 (in Chinese with English abstract).
Ping, H., Chen, H., Thiéry, R., 2013b. Thermodynamic modeling of petroleum inclusions: composition modeling and prediction of the trapping pressure of crude oils. Fluid Phase Equil. 346, 33–44.
Ping, H., Chen, H., Thiéry, R., George, S.C., 2017b. Effects of oil cracking on fluorescence color, homogenization temperature and trapping pressure reconstruction of oil inclusions from deeply buried reservoirs in the northern Dongying Depression, Bohai Bay Basin, China. Mar. Petrol. Geol. 80, 538–562.
Ping, H., Chen, H., Zhai, P., Zhu, J., George, S.C., 2019. Petroleum charge history in the Baiyun depression and Panyu lower uplift in the Pearl River Mouth Basin, northern South China Sea: constraints from integration of organic geochemical and fluid inclusion data. AAPG (Am. Assoc. Pet. Geol.) Bull. 103 (6), 1401–1442.
Ping, H., Li, C., Chen, H., George, S., Gong, S., 2020b. Overpressure release: fluid inclusion evidence for a new mechanism for the formation of heavy oil. Geology 48 (8), 803–807.
Ping, H., Thiéry, R., Chen, H., 2011. Thermodynamic modelling of petroleum inclusions: the prediction of the saturation pressure of crude oils. Geofluids 11 (3), 328–340.
Pironon, J., 2020. Constraining fluid and diagenetic events in sedimentary basins by combining fluid inclusion data with burial models: discussions and recommendations. In: Lecumberri-Sanchez, P., Steele-MacInnis, M., Kontak, D. (Eds.), Fluid and Melt Inclusions: Applications to Geologic Processes: London, Ontario, Canada, Mineralogical Association of Canada Topics in Mineral Sciences, vol. 49, pp. 1–15.
Pironon, J., Bourdet, J., 2008. Petroleum and aqueous inclusions from deeply buried reservoirs: experimental simulations and consequences for overpressure estimates. Geochem. Cosmochim. Acta 72 (20), 4916–4928.
Pironon, J., Canals, M., Dubessy, J., Walgenwitz, F., Laplace-Builhe, C., 1998. Volumetric reconstruction of individual oil inclusions by confocal scanning laser microscopy. Eur. J. Mineral 10 (6), 1143–1150.
Pironon, J., Thiery, R., Ayt Ougougdal, M., Teinturier, S., Beaudoin, G., Walgenwitz, F., 2001. FT-IR measurements of petroleum fluid inclusions: methane, n-alkanes and carbon dioxide quantitative analysis. Geofluids 1 (1), 2–10.
Pironon, J., Thiéry, R., Teinturier, S., Walgenwitz, F., 2000. Water in petroleum inclusions: evidence from Raman and FT-IR measurements, PVT consequences. J. Geochem. Explor. 69–70, 663–668.
Potter II, R.W., 1977. Pressure corrections for fluid-inclusion homogenization temperatures based on the volumetric properties of the system NaCl-H_2O. J. Res. U. S. Geol. Surv. 5 (5), 603–607.
Qi, Z., Liang, B., Deng, R., Du, Z., Wang, S., Zhao, W., 2007. Phase Behavior Study in the Deep Gas-Condensate Reservoir with Low Permeability. EUROPEC/EAGE Conference and Exhibition.
Raffie, H., Tennyson, J., 2003. Optimizing the number of components in tuning the Peng-Robinson Equation-of-State for Trinidad's gas condensates. In: SPE Latin American and Caribbean Petroleum Engineering Conference.
Raimbourg, H., Thiéry, R., Vacelet, M., Ramboz, C., Cluzel, N., Le Trong, E., Yamaguchi, A., Kimura, G., 2014. A new method of reconstituting the P–T conditions of fluid circulation in an accretionary prism (Shimanto, Japan) from microthermometry of methane-bearing aqueous inclusions. Geochem. Cosmochim. Acta 125, 96–109.
Reamer, H.H., Sage, B.H., 1950. Volumetric behavior of oil and gas from a Louisiana Field I. J. Petrol. Technol. 2 (9), 261–268.
Regueira, T., Glykioti, M.-L., Kottaki, N., Stenby, E.H., Yan, W., 2020. Density, compressibility and phase equilibrium of high pressure-high temperature reservoir fluids up to 473 K and 140 MPa. J. Supercrit. Fluids 159, 104781.
Remolina, J.-C.-M.E., Parra, C.-A.C., 2006. Development of a super accelerated successive substitution, new method for saturation pressure calculation in synthetic mixtures and reservoir fluids. C.T. F Ciencia, Tecnol., Futuro 3 (2), 83–93.
Riazi, M.R., Al-Sahhaf, T.A., 1996. Physical properties of heavy petroleum fractions and crude oils. Fluid Phase Equil. 117 (1–2), 217–224.
Riemens, W., Schulte, A., de Hong, L., 1988. Birba field PVT variations along the hydrocarbon column and confirmatory field tests. J. Petrol. Technol. 40 (1), 83–88.
Roedder, E., 1984. Fluid Inclusions. Reviews in Mineralogy, 12. Mineralogical Society of America, Washington, p. 646.
Sage, B.H., Olds, R.H., 1947. Volumetric behavior of oil and gas from several San Joaquin Valley fields. Transactions of the AIME 170 (1), 156–173.
Schowalter, T.T., 1979. Mechanics of secondary hydrocarbon migration and entrapment. AAPG (Am. Assoc. Pet. Geol.) Bull. 63 (5), 723–760.
Shokir, E.M.E.-M.B., 2008. Dewpoint pressure model for gas condensate reservoirs based on genetic programming. In: CIPC/SPE Gas Technology Symposium 2008 Joint Conference.
Siljeström, S., Volk, H., George, S., 2021. Using ToF-SIMS analyses for analysing individual oil inclusions of different fluorescence colours in a single quartz crystal from the Barrandian (Czech Republic). Org. Geochem. 164, 104354.
Siljeström, S., Volk, H., George, S.C., Lausmaa, J., Sjövall, P., Dutkiewicz, A., Hode, T., 2013. Analysis of single oil-bearing fluid inclusions in mid-Proterozoic sandstones (Roper Group, Australia). Geochem. Cosmochim. Acta 122 (0), 448–463.
Silverman, R.W., Hill, C.R., Gas Processors, A., 1997. The Conversion of Natural Gas to Liquid Fuels Using the SASOL Slurry Phase Distillate Process. Gas Processors Association - Seventy-Sixth Annual Convention, Proceedings, pp. 239–241.
Sportisse, M., Barreau, A., Ungerer, P., 1997. Modeling of gas condensates properties using continuous distribution functions for the characterisation of the heavy fraction. Fluid Phase Equil. 139 (1–2), 255–276.
Stainforth, J.G., 2009. Practical kinetic modeling of petroleum generation and expulsion. Mar. Petrol. Geol. 26 (4), 552–572.
Standing, M.B., 1979. A Set of equations for computing equilibrium ratios of a crude oil/natural gas system at pressures below 1,000 psia. J. Petrol. Technol. 31 (9), 1193–1195.
Stenby, E.H., Christensen, J.R., Knudsen, K., Leibovici, C., 1996. Application of a Delumping Procedure to Compositional Reservoir Simulations. SPE Annual Technical Conference and Exhibition.
Sun, C.-Y., et al., 2012. Experiments and modeling of volumetric properties and phase behavior for condensate gas under ultra-high-pressure conditions. Ind. Eng. Chem. Res. 51 (19), 6916–6925.
Teinturier, S., Pironon, J., Walgenwitz, F., 2002. Fluid inclusions and PVTX modelling: examples from the garn formation in well 6507/2-2, haltenbanken, mid-Norway. Mar. Petrol. Geol. 19 (6), 755–765.
Thiéry, R., 2006. Thermodynamic modelling of aqueous CH_4-bearing fluid inclusions trapped in hydrocarbon-rich environments. Chem. Geol. 227 (3–4), 154–164.
Thiéry, R., Pironon, J., Walgenwitz, F., Montel, F., 2000. PIT (Petroleum Inclusion Thermodynamic): a new modeling tool for the characterization of hydrocarbon fluid inclusions from volumetric and microthermometric measurements. J. Geochem. Explor. 69–70, 701–704.
Thiéry, R., Pironon, J., Walgenwitz, F., Montel, F., 2002. Individual characterization of petroleum fluid inclusions (composition and P-T trapping conditions) by microthermometry and confocal laser scanning microscopy: inferences from applied thermodynamics of oils. Mar. Petrol. Geol. 19 (7), 847–859.
Thomas, F.B., Andersen, G., Bennion, D.B., 2006. Gas Condensate Reservoir Performance: Part I - Fluid Characterization. Canadian International Petroleum Conference.
Thomassen, P., Pedersen, K.S., Fredenslund, A., 1987. Adjustment of C_{7+} Molecular Weights in the Characterization of Petroleum Mixtures Containing Heavy Hydrocarbons. SPE, 16036. MS.
Tissot, B.P., Welte, D.H., 1984. Petroleum Formation and Occurrence. Springer-Verlag, New York, p. 699.
Tseng, H.-Y., Burruss, R.C., Onstott, T.C., Omar, G., 1999. Paleofluid-flow circulation within a Triassic rift basin: evidence from oil inclusions and thermal histories. Geol. Soc. Am. Bull. 111 (2), 275–290.
Tseng, H.-Y., Pottorf, R.J., 2002. Fluid inclusion constraints on petroleum PVT and compositional history of the Greater Alwyn–South Brent petroleum system, northern North sea. Mar. Petrol. Geol. 19 (7), 797–809.
Valiollahi, S., Kavianpour, B., Raeissi, S., Moshfeghian, M., 2016. A new Peng-Robinson modification to enhance dew point estimations of natural gases. J. Nat. Gas Sci. Eng. 34, 1137–1147.
Vega, L., Barrufet, M.A., 2005. Analysis of a non-volumetric gas-condensate reservoir using a generalized material balance equation with fluid properties from an equation of state. J. Petrol. Sci. Eng. 48 (1–2), 105–119.
Vityk, M.O., Pottorf, R.H., Chimenti, R.J., 123, 2002. Method to Evaluate the Hydrocarbon Potential of Sedimentary Basins from Fluid Inclusions. United States Patent Application, USA.
Vogel, J.L., Yarborough, L., 1980. The Effect of Nitrogen on the Phase Behavior and Physical Properties of Reservoir. SPE/DOE Enhanced Oil Recovery Symposium. SPE, Tulsa, Oklahoma, p. 8815. MS.
Volk, H., Fuentes, D., Fuerbach, A., Miese, C., Koehler, W., Bärsch, N., Barcikowski, S., 2010. First on-line analysis of petroleum from single inclusion using ultrafast laser ablation. Org. Geochem. 41 (2), 74–77.
Volk, H., Horsfield, B., Mann, U., Suchý, V., 2002. Variability of petroleum inclusions in vein, fossil and vug cements—a geochemical study in the Barrandian Basin (Lower Palaeozoic, Czech Republic). Org. Geochem. 33 (12), 1319–1341.
Volk, H., George, S.C., 2019. Using petroleum inclusions to trace petroleum systems – a review. Org. Geochem. 129, 99–123.
Wang, L.S., Gmehling, Jürgen, 1999. Improvement of SRK equation of state for vapor-liquid equilibria of petroleum fluids. AIChE J. 45 (5), 1125–1134.
Williams, C.A., Zana, E.N., Humphrys, G.E., 1980. Use of the Peng-Robinson Equation of State to Predict Hydrocarbon Phase Behavior and Miscibility for Fluid Displacement, SPE/DOE Enhanced Oil Recovery Symposium. Society of Petroleum Engineers, Tulsa, Oklahoma.
Wu, R., Rosenegger, L., 1999. Intergrated oil PVT data characterization-lessons from four case histories. J. Can. Petrol. Technol. 38 (13), 97, 05.
Yan, W., Wang, L.-K., Yang, L.-Y., Guo, T.-M., 2001. A systematic experimental study on the phase behavior of complex fluid mixtures up to near-critical region. Fluid Phase Equil. 190 (1), 159–178.
Yang, T., Chen, W.D., Guo, T.M., 1997. Phase behavior of a near-critical reservoir fluid mixture. Fluid Phase Equil. 128 (1–2), 183–197.

Yang, Y., Lun, Z., Wang, R., Hu, W., 2020. Non-equilibrium Phase Behavior in Gas Condensate Depletion Experiments, vol. 506. Fluid Phase Equilibria.
Yushchenko, T.S., Brusilovsky, A.I., 2015. Modeling of PVT-Properties of Natural Gas Condensate Mixtures Adjusted for Presence of Residual Water in Collector. SPE Russian Petroleum Technology Conference.
Yushchenko, T.S., Brusilovsky, A.I., 2016. Mathematical modeling of gas-condensate mixture PVT-properties including presence of brine in reservoir. Fluid Phase Equil. 409, 37–48.
Zhang, A., Fan, Z., Zhao, L., 2020. An investigation on phase behaviors and displacement mechanisms of gas injection in gas condensate reservoir. Fuel 268.
Zhang, Z., Greenwood, P., Zhang, Q., Rao, D., Shi, W., 2012. Laser ablation GC–MS analysis of oil-bearing fluid inclusions in petroleum reservoir rocks. Org. Geochem. 43 (0), 20–25.
Zhong, Z., Liu, S., Kazemi, M., Carr, T.R., 2018. Dew point pressure prediction based on mixed-kernels-function support vector machine in gas-condensate reservoir. Fuel 232, 600–609.
Zurita, R.A.A., William, D., McCain, J., 2002. An efficient tuning strategy to calibrate cubic EoS for compositional simulation. In: SPE Annual Technical Conference and Exhibition. SPE, San Antonio, Texas, 77382.
Jamaluddin, A.K.M., Joshi, N., Iwere, F. and Gurpinar, O., 2002. An investigation of asphaltene instability under nitrogen injection, SPE International Petroleum Conference and Exhibition in Mexico.